ISSN 1674-1056
http://cpb.iphy.ac.cn
http://iopscience.iop.org/cpb
中国物理 B
Chinese Physics
中国物理 Chinese Physics B

Neutron-based characterization techniques for lithium-ion battery research

Enyue Zhao(赵恩岳)[1,2], Zhi-Gang Zhang(张志刚)[1,2], Xiyang Li(李西阳)[2], Lunhua He(何伦华)[1,2,4], Xiqian Yu(禹习谦)[2], Hong Li(李泓)[2], Fangwei Wang(王芳卫)[1,2,3,4]

Citation: Chin. Phys. B . 2020, 29(1): 018201 . **doi:** 10.1088/1674-1056/ab5d07
Journal homepage: http://cpb.iphy.ac.cn; http://iopscience.iop.org/cpb

What follows is a list of articles you may be interested in

Parameter identification and state-of-charge estimation approach for enhanced lithium-ion battery equivalent circuit model considering influence of ambient temperatures

Hui Pang(庞辉), Lian-Jing Mou(牟联晶), Long Guo(郭龙)
Chin. Phys. B . 2019, 28(10): 108201 . **doi:** 10.1088/1674-1056/ab3af5

Artificial solid electrolyte interphase based on polyacrylonitrile for homogenous and dendrite-free deposition of lithium metal

Hang-Yu Xu(徐航宇), Quan Li(李泉), Hong-Yi Pan(潘弘毅), Ji-Liang Qiu(邱纪亮), Wen-Zhuo Cao(曹文卓), Xi-Qian Yu(禹习谦), Hong Li(李泓)
Chin. Phys. B . 2019, 28(7): 078202 . **doi:** 10.1088/1674-1056/28/7/078202

First-principles insight into Li and Na ion storage in graphene oxide

Shu-Ying Zhong(钟淑英), Jing Shi(石晶), Wen-Wei Luo(罗文崴), Xue-Ling Lei(雷雪玲)
Chin. Phys. B . 2019, 28(7): 078201 . **doi:** 10.1088/1674-1056/28/7/078201

Improved electrochemical performance of $Li(Ni_{0.6}Co_{0.2}Mn_{0.2})O_2$ at high charging cut-off voltage with $Li_{1.4}Al_{0.4}Ti_{1.6}(PO_4)_3$ surface coating

Yi Wang(王怡), Bo-Nan Liu(刘柏男), Ge Zhou(周格), Kai-Hui Nie(聂凯会), Jie-Nan Zhang(张杰男), Xi-Qian Yu(禹习谦), Hong Li(李泓)
Chin. Phys. B . 2019, 28(6): 068202 . **doi:** 10.1088/1674-1056/28/6/068202

Influence of carbon coating on the electrochemical performance of SiO@C/graphite composite anode materials

Hao Lu(陆浩), Junyang Wang(汪君洋), Bonan Liu(刘柏男), Geng Chu(褚赓), Ge Zhou(周格), Fei Luo(罗飞), Jieyun Zheng(郑杰允), Xiqian Yu(禹习谦), Hong Li(李泓)
Chin. Phys. B . 2019, 28(6): 068201 . **doi:** 10.1088/1674-1056/28/6/068201

TOPICAL REVIEW — Advanced calculation & characterization of energy storage materials & devices at multiple scale

Neutron-based characterization techniques for lithium-ion battery research*

Enyue Zhao(赵恩岳)[1,2], Zhi-Gang Zhang(张志刚)[1,2], Xiyang Li(李西阳)[2], Lunhua He(何伦华)[1,2,4], Xiqian Yu(禹习谦)[2], Hong Li(李泓)[2], and Fangwei Wang(王芳卫)[1,2,3,4,†]

[1] *Songshan Lake Materials Laboratory, Dongguan* 523808, *China*
[2] *Beijing National Laboratory for Condensed Matter Physics, Institute of Physics, Chinese Academy of Sciences, Beijing* 100190, *China*
[3] *School of Physical Sciences, University of Chinese Academy of Sciences, Beijing* 101408, *China*
[4] *China Spallation Neutron Source (CSNS), Dongguan* 523808, *China*

(Received 31 October 2019; revised manuscript received 24 November 2019; published online 29 November 2019)

During the past decades, Li-ion batteries have been one of the most important energy storage devices. Large-scale energy storage requires Li-ion batteries which possess high energy density, low cost, and high safety. Other than advanced battery materials, in-depth understanding of the intrinsic mechanism correlated with cell reaction is also essential for the development of high-performance Li-ion battery. Advanced characterization techniques, especially neutron-based techniques, have greatly promoted Li-ion battery researches. In this review, the characteristics or capabilities of various neutron-based characterization techniques, including elastic neutron scattering, quasi-elastic neutron scattering, neutron imaging, and inelastic neutron scattering, for the related Li-ion-battery researches are summarized. The design of *in-situ/operando* environment is also discussed. The comprehensive survey on neutron-based characterizations for mechanism understanding will provide guidance for the further study of high-performance Li-ion batteries.

Keywords: Li-ion battery, neutron scattering, characterization technique

PACS: 82.47.Aa, 82.45.Fk **DOI:** 10.1088/1674-1056/ab5d07

1. Introduction

Energy storage has been one of the major worldwide concerns over the past decades. Due to the advantage of high energy density, lithium-ion batteries (LIBs) have become the dominant energy storage devices for micro-electronic products since 1990s.[1–5] LIBs with higher energy density and lower cost are needed to further meet the requirement of large-scale energy storage, such as smart grids and electric vehicles. The researchers from both industry and scientific community are paying attention to the optimization and design of high-performance LIBs.[6–9] Since LIBs are essentially electrochemical cells which are composed of electrodes and electrolyte, understanding the physical/chemical nature of these components as well as the internal electrochemical process and degradation mechanism of LIBs is a prerequisite for breakthroughs on their electrochemical performance.

During the past years, various advanced characterization tools, such as synchrotron-based x-ray diffraction/spectroscopy/microscopy, (scanning) transmission electron microscopy, etc., have played a critical role in promoting the mechanism understanding for LIBs.[10–14] Among all the probes, neutron-based characterization techniques have unique advantages due to the complementary scattering cross-sections of neutron compared to those of x-ray and electron. Specifically, neutron is more sensitive to light atoms (e.g., H, Li, O) than x-ray/electron and has the ability in distinguishing the neighboring elements (e.g., Ni, Mn, Co). On the other hand, neutron has strong penetrability which is favorable for the nondestructive *in-situ/operando* measurement of commercial LIBs. Based on these characteristics, neutron-based characterization techniques, including neutron powder diffraction (NPD), neutron pair distribution function (NPDF), small angle neutron scattering (SANS), neutron reflection (NR), neutron imaging (NI), neutron depth profile (NDP), quasi-elastic neutron scattering (QENS), and inelastic neutron scattering (INS), have made great contribution to the fundamental research and industrial application of LIBs.

Here, we present a review of recent progress in neutron-based characterization for Li-ion battery research (Fig. 1). Special attention is focused on how various neutron-based characterization techniques are being used and what characteristic or capability they possess. Several case studies are employed to illustrate how neutron-based characterization has advanced the Li-ion battery research. We first briefly introduce the fundamental demands and challenges for LIBs. Then, detailed discussions regarding the recent research discoveries, such as Li-storage/diffusion mechanism, structure evolution,

*Project supported by the National Key R&D Program of China (Grant No. 2016YFA0401503), the National Materials Genome Project of China (Grant No. 2016YFB0100106), and the National Natural Science Foundation of China (Grant No. 11675255).

†Corresponding author. E-mail: fwwang@iphy.ac.cn

© 2020 Chinese Physical Society and IOP Publishing Ltd

cell degradation mechanism, etc., based on various neutron-based characterizations are presented. Meanwhile, the design and significance of the *in-situ/operando* neutron-based characterization are also discussed. Finally, concluding remarks and perspectives on how neutron-based characterization techniques can be further applied for the development of high-energy-density LIBs are presented.

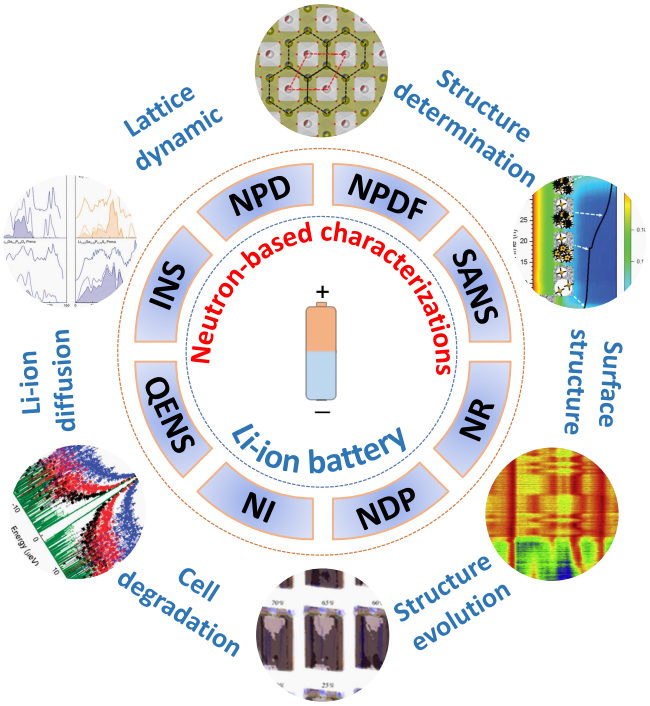


Fig. 1. An overview of various neutron-based characterization techniques in promoting the development of Li-ion battery researches (NPD: neutron powder diffraction, NPDF: neutron pair distribution function, SANS: small angle neutron scattering, NR: neutron reflection, NDP: neutron depth profile, NI: neutron imaging, QENS: quasi-elastic neutron scattering, INS: inelastic neutron scattering).

2. Demands and challenges for Li-ion batteries

Superior properties, including higher energy density, higher power density, longer cycle life, lower cost, higher safety, better eco-friendly, etc., have become the development goals for the next-generation LIBs. Achieving all these goals makes it essential to find better electrode and electrolyte materials as well as to design a more optimal battery cell. Although numerous optimization strategies have significantly advanced the overall performance of LIBs, in-depth insights of their performance-related mechanisms are needed to further guide Li-ion battery fundamental research and commercial applications. The intrinsic characteristics of LIBs determine that the challenges associated with electrochemical performance are mainly focused on the following aspects: battery materials, electrochemical reactions, and cell fabrication design.

The Li-storage capability of LIBs is closely associated with the structural stability of the electrode materials. For instance, the development of high-capacity cathode materials, such as high-voltage $LiCoO_2$, Ni-rich ternary transition metal (TM) oxides, and Co-free Li-rich TM oxides, largely enhances the energy density of LIBs. However, the unfavorable structure evolution (e.g., irreversible phase transition) of these cathode materials upon the (de)lithiation process limits their cycle life.[15–18] The similar scenario could also be found in silicon or silicon/carbon composite anodes which show much higher specific capacity than that of traditional graphite materials.[19] Specifically, the large structure and volume changes induced by the alloying reaction of Li with silicon usually lead to the mechanical failure of the electrodes and make it difficult for silicon or its composite electrode to achieve both ultrahigh capacity and good cycle stability. In addition, the thermodynamic and electrochemical/chemical stabilities of the liquid electrolyte with respect to the cathode and anode materials have important effects on the cycle life and safety of LIBs. Upon the charging/discharging processes, there are always inevitable side reactions, that is the formation of solid electrolyte interface (SEI) layer, on the interface between the electrodes and electrolytes. Since the SEI layer is electronically insulating, a uniform and dense passivating SEI layer would retard the further oxidation or reduction of the liquid electrolytes, and thus promote the surface stability of the electrodes.[20,21] Usually, the uncontrolled growth of the SEI layer would also not only cause constant consumption of the electrolyte but also lead to large electrode polarization for the electrochemical reactions. This meanwhile illustrates why the surface modification engineering of the electrodes as well as the optimization of the liquid electrolytes is always significant.[20,22–25]

Rechargeable LIBs with Li metal as the anode, usually also called Li-metal batteries, can obvious improve their energy density. However, safety problems caused by the growth of Li dendritic seriously restrict the practical application of Li-metal batteries, though lots of modification strategies have significantly advance the improvement of their overall performance.[26,27] It is worth noting that the application of solid-state electrolytes (i.e., all-solid-state batteries) has been regarded as one of the most effective strategies to enable the application of Li-metal anode. Nowadays, many kinds of solid-state electrolytes, such as glasses and glass ceramics, Li_6PS_5Cl and isostructural compounds, $Li_{14}Zn(GeO_4)_4$/$Li_{4-x}Ge_{1-x}P_xS_4$ and their analogues, NASICON and garnets-type oxides, have been developed, and their ionic conductivity was also significantly improved by various optimization methods.[28,29] It has been reported that the interfacial instability between Li metal and solid-state electrolytes is the main challenge to be overcame for all-solid-state batteries. Furthermore, the ionic conductivity of the solid-state electrolytes is still needed to be further improved to meet the high-power-density requirement for all-solid-state LIBs. In addition, although the configuration for LIBs (consist of only cathodes, anodes, electrolytes, and several electrochemical inert components) is deceptively simple, it is critical to care-

fully combine these components to achieve the superior overall performance mentioned at the beginning. In the process of solving the above challenges and propelling the development of high-energy-density Li-ion batteries, neutron-based characterization combined with the state-of-the-art *in situ/operando* methods has played an important role.

3. Neutron-based characterization techniques

3.1. Neutron powder diffraction

Powder diffraction is a typical characterization tool to observe the crystal structure information for polycrystalline materials. Since most electrode and electrolyte materials in LIBs are well crystalline, NPD has been widely used for their crystal structure analysis. NPD relies on the coherent-interference pattern (i.e., Bragg peak) that is scattered from well-defined lattice planes in polycrystalline materials. The phase composition, microscopic stress, structure distortion, lattice defect, atomic occupation, and even modest dynamical information (e.g., Li-ion diffusion pathways) of materials can be obtained from the measured NPD patterns. The accuracy of these structure information is highly dependent on the resolution of the diffractometer as well as the refinement process. It also should be noted that the introduction of proper isotopes, such as ^{7}Li, in the samples can improve the overall quality of the measured NPD data. In addition, compared with other neutron-based characterizations, NPD technique has the advantage of essential simplicity, which makes it the prime candidate for *in-situ/operando* researches of LIBs.

The electrochemical performance of cathode materials is closely correlated with their crystal structure. NPD plays a critical role in deciphering their structure–property relation. Take commercialized $LiFePO_4$ electrode material as an example, the intriguing correlation between its crystal chemistry and rate capability is clearly revealed by NPD. Using NPD, Delacourt *et al.* for the first time provided the experimental evidence of a solid solution Li_xFePO_4 ($0 \leq x \leq 1$) at high temperature (450 °C), and two new metastable phases with compositions $Li_{0.75}FePO_4$ and $Li_{0.5}FePO_4$ at room temperature.[34] They also demonstrated that these metastable phases pass through another metastable phase, that is $Li_{\sim 0.67}FePO_4$, during the cooling process.[35] NPD results indicated that the Li–O bond in $Li_{\sim 0.67}FePO_4$ is longer than that in $LiFePO_4$, the discrepant bond length results in the metastability of the intermediate phase as well as the two-phase mechanism in the $LiFePO_4$ system.[34,35] Since the rate capability of the $LiFePO_4$ electrode is associated with this metastable phase, the understanding of its transition mechanism is favorable for improving the power density of $LiFePO_4$ material. In addition, NPD characterization also made a breakthrough in visualize the Li-ion diffusion path in $LiFePO_4$. By combining high-temperature NPD with the maximum entropy analysis method, Nishimura *et al.* presented experimental evidence for a curved one-dimensional path for Li-ion migration.[36] This important experiment result not only verifies the previous computational predictions, but also highlights the effect of Li-Fe anti-site defect on the one-dimensional migration channels. Based on the advanced NPD technique, numerous researches regarding the impact of synthesis method, heteroatom doping, composition, and particle size on the anti-site defect, were conducted, which is of great importance for the development of high-performance $LiFePO_4$ electrode.[35,37,38] Lots of new polyanion-based cathode materials, such as $LiM_xFe_{1-x}PO_4$ (M = Mn, Co), fluoride-phosphates (Li_2MPO_4F, M = Fe, Mn, Co, Ni), etc., were developed in the meantime thanks to the NPD characterization.[39] Besides the high-safety olive positive electrodes, NPD also made vital contribution to the development of high-voltage spinel electrodes and high-energy density layered cathode oxides. Using NPD, Liu *et al.* suggested that the occurrence and degree of Ni/Mn disordering are closely related with the formation of oxygen vacancies in $LiNi_{0.5}Mn_{1.5}O_4$ samples, and researchers found that the transition-metal ordering in $LiNi_{0.5}Mn_{1.5}O_4$ is determined by the synthesis process.[40] For the reaction mechanisms in spinel $LiMn_2O_4$, by employing *operando* NPD, Song *et al.* proposed that there are solid-solution regions within both cubic and tetragonal spinel phases other than a continuous phase transition between them.[41] Similar to that in olivine-type cathode materials, cation mixing is the most recognizable intrinsic defect type in the layered cathode oxides, especially in Ni-rich layered oxides, the existence of which has tremendously hindered the cycle stability and rate capability of the electrode materials. Using NPD, Zhao *et al.* systematically studied the impact of synthesis method and elements doping on the Li/Ni mixing in layered cathode oxides.[42–44] Also, a research work conducted by Li *et al.* suggested that the halogen substitution could facilitate the neighboring Li and Ni atoms to exchange their sites and form the stable local octahedron of halide, thus enhancing the electrochemical performance of the Ni-rich layered cathode.[45] For elucidating the structure evolution and reaction mechanism of layered cathodes upon the de-/lithiation process, *operando* NPD is a powerful tool. For instance, using *operando* NPD, Goonetilleke *et al.* indicated that a higher Ni content in $Li(Ni_xMn_yCo_z)O_2$ ($x + y + z = 1$) will lead to greater structure change upon cycling,[46] while Chen *et al.* revealed the underlying phase transformations mechanism which is responsible for the initiation and intensification of particle cracking in the Li-rich layered oxides.[47] In addition, NPD advanced the structure and mechanism revelations of many new positive electrode materials for LIBs.[30,48,49] Zhao *et al.* demonstrated the robust oxygen framework structure of cation-disordered Li-rich cathode oxides upon the de-lithiation process (Fig. 2(a)),[30] while Liu *et al.* revealed the ion exchange synthesis mechanism of

$Li_2Mg_2P_3O_9N$ cathode material.[49] Meanwhile, for the negative electrode materials, such as graphite, carbon, $Li_4Ti_5O_{12}$, NPD has been employed to detect their crystal structure, structure evolution, redox reaction mechanisms, etc., making great progress in promoting their practical application.[50–52]

As a powerful tool, NPD largely favors the fundamental study of solid-state electrolytes. The intrinsic crystal structure of solid-state electrolytes as well as their Li-ion conductivity and dynamic can both be reliably evaluated via NPD. Due to the excellent chemical/thermal stability and good electrochemical inertness against Li metal, Li oxide garnets with cubic structure have been considered as the promising candidates for solid-state electrolytes in Li-ion and Li metal batteries. To study the phase-formation process of $Li_7La_3Zr_2O_{12}$ (LLZO) and provide an in-depth understanding for its fabrication procedures, *in situ* NPD was applied in the research work conducted by Rao and co-workers (Figs. 2(b) and 2(c)).[31] The *in situ* NPD indicated that there is an effect of the partial melting of precursors on the formation of the fast-ion conducting phase, which suggested that the formation of LLZO originates from the decomposition of a partial carbonate melt during the heating process (Figs. 2(b) and 2(c)).[31] The lithium ordering and ionic conductivity of LLZO are easily affected by the cooling rate. Since the ion conductivity of LLZO at room temperature is still lower than that of the other superionic conductors (e.g., $Li_{10}GeP_2S_{12}$, $Li_{1+x}Al_xTi_{2-x}(PO_4)_3$), strategies, such as elements doping, are being used to modify its Li-ion conductivity. NPD played an important role in illustrating how elements doping influences the crystal structure, thus improving the ion conductivity of LLZO.[53] Using NPD, Meesala *et al.* found that the optimized ion conductivity in ternary-doped garnet structure $Li_{6.65}Ga_{0.05}La_{2.95}Ba_{0.05}Zr_{1.75}Ta_{0.25}O_{12}$ is ascribed to the dense microstructure and increased Li-ion occupancy in the tetrahedral-24d_{Li1} site.[54] Wagner *et al.* proposed that the introduction of Bi^{5+} into LLZO can result in the increase of the unit-cell parameters, which is associated with the observed fast Li ion dynamics in $Li_{7-x}La_3Zr_{2-x}Bi_xO_{12}$.[55] Meanwhile, Orera *et al.* studied the effect of H content on the crystal structure of LLZO by employing NPD, which is significant for the optimization of their chemical stability.[56] Apart from the oxide electrolytes with d^0-valence-states transition metal, including $La_{2/3-x}Li_{3x}TiO_3$, $Li_7La_3Zr_2O_{12}$, and $Li_xLa_{(1-x)/3}NbO_3$, Takami *et al.* developed a new lithium-intercalated oxide La-Li-Co-O with a lithium-ion conductivity of 7×10^{-5} S·cm^{-1} at 140 °C. By combing NPD with maximum entropy method, they found a quasi-one-dimensional pathway for lithium diffusion which should be responsible for the realization of lithium-ion conduction in La-Li-Co-O oxides.[57] In addition to the garnet-type oxide superionic, NPD also advanced the development of other classic solid-state electrolytes (e.g., $Li_{1+x}Al_xTi_{2-x}(PO_4)_3$, lithium thiophosphates).[58] For instance, Dietrich *et al.* revealed the origin of the low ionic conductivity in $Li_2P_2S_6$ via NPD.[59] Specifically, $Li_2P_2S_6$ has $P_2S_6^{2-}$ polyhedral units with edge-sharing PS_4 tetrahedra and only one-dimensional diffusion pathways with localized distributed Li–Li atomic pairs, which is not favorable for the migration of Li-ion.[59] In the research work regarding other new superionic, such as Li_4PS_4I, $Li_6CuB_4O_{10}$, and lithium-rich anti-perovskites, NPD has certainly been an essential characterization for understanding their structure–property relation.[60–62]

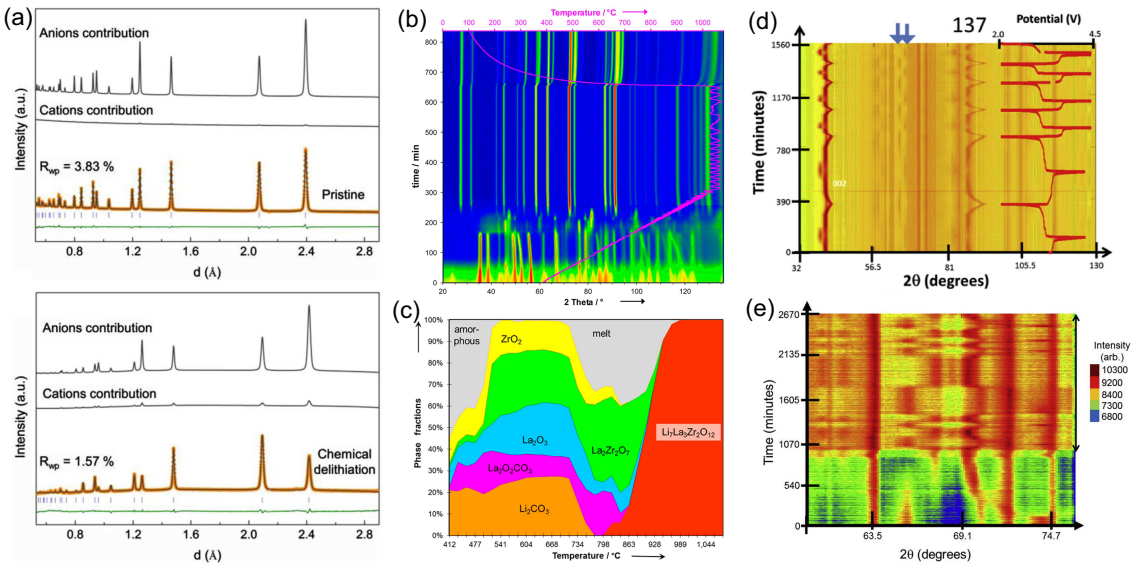


Fig. 2. (a) Rietveld refinement of the NPD patterns and calculated cations/anions diffraction patterns for the pristine and Li extracted cation-disordered Li-rich cathode oxide structure. Reproduced with permission.[30] Copyright 2019, Elsevier. (b) Two-dimensional intensity contour map of diffraction patterns during the formation of $Li_7La_3Zr_2O_{12}$ material, (c) Weight fractions of the phases present in the $Li_7La_3Zr_2O_{12}$ sample during the heating determined using Rietveld analysis of the data shown in panel (b). Reproduced with permission.[31] Copyright 2015, American Chemical Society. (d) *In operando* NPD patterns for the calendar aged battery. Reproduced with permission.[32] Copyright 2017, Elsevier. (e) A contour plot of *in operando* NPD data for the phase evolution of $LiFePO_4$ in a commercial battery. Reproduced with permission.[33] Copyright 2017, Elsevier.

Understanding the aging behavior, such as the thermal stability, fatigue processes, storage degradation, etc., of commercial LIBs is significant for the optimization of the cell manufacturing technology. NPD combined with *in-situ/operando* experiment method has been the typical characterization tool for the aging mechanism study of commercial LIBs.[32,63–66] Paul *et al.* studied the aging behavior of commercial 18650-type Li-ion battery which consists a $LiFePO_4$ cathode and a graphite anode based on either meso-carbon microbeads (MCMB) or needle coke (NC).[63] Different from the inferior cycle stability and storage capability of the NC-based battery, the cell based on MCMB anode showed only 8% relative capacity loss after 4750 cycles and no capacity loss on storage for two years. The *in situ* NPD results suggested that the loss of active lithium should be responsible for the capacity loss in both cells and no other aging evidence such as the structure degradation of the electrode materials was detected.[63] The similar fatigue mechanism was also found by NPD in a commercial 18650-type cell based on $LiCoO_2$ cathode in the research work conducted by Dolotko *et al.*[66] Interestingly, Lee *et al.* found that the loss of active lithium is also the main reason that results in the inferior energy storage capability of the commercial battery.[65] For the thermal stability of commercial battery, Baran *et al.* probed the structure response of the electrode materials in a broad temperature range 4–360 K via high-resolution NPD.[64] They suggested that there is an obvious effect of the temperature on the equilibrium states of electrode materials during de-/lithiation process. Meanwhile, Goonetilleke and co-workers studied the relation between cycling history and structural evolution in a commercial 26650-type battery using *operando* NPD (Fig. 2(d)).[32] It was indicated that the battery cycling history has a determining effect on the graphite/lithiated graphite (Li_xC_6 or Li_yC) reflections as well as the electrode response to the applied current. As is well known, electrode materials usually show a different electrochemical behavior in a full-cell configuration compared with that in a half-cell system. Thus, it is of great importance to understand the structure evolution of electrodes under real conditions.[33,67–69] The *in situ* NPD was used to probe the structural evolution of the electrode materials in an ICR 10440 commercial cylindrical cell based on a three-phase mixture of Li(Ni, Mn, Co)O_2, $LiCoO_2$, and $LiMn_2O_4$ as the cathode and graphite as the anode. Nazer *et al.* found that there is a underwent structural change for the graphite anode, and the partial lithium depletion upon the charging process will lead to the volume shrinkage for Li(Ni, Mn, Co)O_2 compared with (Ni, Mn)-free $LiCoO_2$ electrode.[67] In another research work conducted by Bobrikov *et al.*, the structure and phase composition in a commercial lithium-ion battery with $LiNi_{0.8}Co_{0.15}Al_{0.05}O_2$ cathode was studied using *in situ* NPD.[68] It was shown that the anode composition evolution is highly dependent on the charge rate and no phase separation of the cathode materials was obtained in the whole voltage range. For the typical two-phase reaction material $LiFePO_4$, *operando* NPD revealed its unusual phase evolution after the application of a thermal step and a high charge/discharge current density (Fig. 2(e)).[33] The two-phase reaction ($LiFePO_4$ to $FePO_4$) appeared later during the charging process with the increase of the current density and temperature, and the same scenario was observed for the $FePO_4$ to $LiFePO_4$ transition during the discharging process, suggesting that the electrode transformation is dependent on the battery's history, current, or temperature.[33] Since graphite is a frequently-used anode material for commercial batteries, probing the lithium concentration in it is of importance for the improvement of the cell overall performance.[70,71] Zinth and co-workers explored the formation of lithium gradients in the graphite anode of a commercial 18650-type cell upon cycling via *in situ* NPD.[70] The NPD data indicated that there is a formation of inhomogeneity in the graphite anode, which will become more pronounced at higher discharging rates.[70] However, the observed inhomogeneity would appear at very low current density (C/10) at the relative low temperature.

3.2. Neutron total scattering

Local (or short-range) structure of electrode materials usually has significant effect on their performance. As mentioned above, NPD, in which only Bragg peaks are considered, is applied to analyze the average (or long-range) structure of materials. Neutron total scattering, including both Bragg and diffuse scatterings, combined with pair distribution function (PDF) analysis method is a powerful tool to detect the structure of materials on a local scale. In this regard, NPDF is of great importance for the structure studies of nano materials, amorphous materials, or polycrystalline materials without good crystallinity. Different from NPD technique, NPDF, which is Fourier transformed from the neutron total scattering data, directly detects the structure information of materials in the real space. The real-space structure information, such as the interatomic distances, atomic coordination numbers, etc., of materials can be observed from the NPDF spectra. Specifically, the PDF peak position, intensity, width, and attenuation represent the average separation of atomic pairs, the coordination number, dynamic disorder, and structural coherence, respectively. Similar to NPD data, NPDF data can also be refined using a "small box" (unit cell) or "big-box" (supercell)

model to obtain more detailed and accurate structure information.

Based on the advantage of NPDF in exploring the local structure of electrode materials, numerous significant researches regarding local structure of LIBs have been conducted. For typical layered transition metal cathode materials, such as $LiNi_{0.5}Mn_{0.5}O_2$ and $LiNi_xMn_yCo_zO_2$, a local ordered structure easily forms in the transition metal layer due to the difference of cationic radius and their valence states. By employing NPDF, Grey's group systematically studied the cation ordering structure in layered cathode oxides and their correlation with electrochemical properties.[72] NPDF analysis indicated that there are differences in the local transition metal arrangements between $Li(Ni_{0.5}Mn_{0.5})O_2$ and $Na(Ni_{0.5}Mn_{0.5})O_2$, suggesting the effect of alkali metal ions on the arrangement of the transition metal layer in layered oxides.[72–74] It was also found that Mn atoms tend to be surrounded by Ni atoms in the first coordination shell, and Ni/Mn cations show a clear preference for ordering in zigzags rather than in chains in the second coordination shell in $Li(Ni_{0.5}Mn_{0.5})O_2$ (no Li atoms in the transition metal layer).[72] Furthermore, by selecting $^6Li(NiMn)_{0.5}O_2$, $^7Li(NiMn)_{0.5}O_2$, and $^7Li(NiMn)_{0.5}O_2$ enriched with ^{62}Ni as the model compounds (10% Li/Ni disordering), NPDF analysis revealed that the different M–O bond lengths (1.93 Å for Mn–O and 2.07 Å for Ni/Li–O) are ascribed to the considerable local distortions in the layers. Reverse Monte Carlo (RMC) calculations of the NPDF patterns indicated that there is a short-range ordered structure (so-called "flower structure" or "honeycomb-like structure") in the transition metal layer which is comprised of $LiMn_6$ and $LiMn_5Ni$ clusters.[73] For ternary layered cathode oxides, by employing NPDF, RMC calculations, and ^6Li MAS NMR, Grey and co-workers suggested that their local environment and short-range ordering are easily influenced by the composition of the materials.[74] NPDF data displayed that there is a nonrandom distribution of Ni and Mn cations in the transition metal layers, where Mn atoms tend to be surrounded by Ni atoms while Co atoms tend to randomly distribute in the first coordination shell. Also, it should be noted that this local ordered structure is directly correlated with the electrochemical reaction mechanisms.[74] In addition, using NPDF tool, Idemoto *et al.* reported that doping or preparation process will affect the local structure, thus determine the electrochemical performance, of ternary layered cathodes.[75,76] For instance, compared with $Li(Mn_{1/3}Ni_{1/3}Co_{1/3})O_2$, the worse cycle stability of $Li(Mn_{1/3}Ni_{1/3}Co_{2/9}Al_{1/9})O_2$ is associated with the varied stacking of the transition metal layers which is induced by the partial substitution of Al for Co.[75] Meanwhile, they found that there is also a difference, such as the precise locations of Li and O, between the average and local structures of high-capacity Li-rich layered cathode oxides.[77] It was reported that the substitution of Al in the spinel $LiMn_2O_4$ will obviously increase its structure stability and cycle performance.[78] To reveal the mechanism, NPDF was performed for the structure study of $LiMn_2O_4$ and $LiMn_{1.8}Al_{0.2}O_4$. It was observed that the distortion parameter of AlO_6 was smaller than that of MnO_6, highlighting the role of Al substitution in mitigating the distortion of the metal-oxygen octahedra.[78]

In addition, NPDF played a critical role in promoting the understanding of lattice oxygen redox (l-OR) mechanism in Li-rich cathode oxides. Since l-OR is essential for achieving the ultrahigh capacity in Li-rich cathode oxides, understanding the oxygen lattice evolution upon oxygen redox is of significant importance. Neutron total scattering, which can detect both local and average structures and is sensitive to light oxygen atoms, is undoubtedly a suitable tool for the research mentioned above. Using *ex situ* NPDF, Zhao *et al.* studied the oxygen lattice evolution of $Li_{1.2}Mn_{0.54}Ni_{0.13}Co_{0.13}O_2$ at different electrochemical states.[79] NPDF and NPD data indicated that, during the l-OR process in Li-rich layered oxides, no obvious average structure change was detected but a significant local oxygen lattice distortion was observed (Fig. 3).[79] It was also found that the oxygen lattice distortion is highly dependent on the cation species. These findings not only deepen the understanding of l-OR mechanisms, but also highlight the importance of the local structure and multi cations in stabilizing the l-OR in Li-rich layered cathode oxides. NPDF was further performed to detect the evolution of O–O atomic pairs in cation-disordered Li-rich cathode oxides upon electrochemical cycling.[80] Compared with Li-rich layered cathode oxides, a relative stable oxygen lattice structure was obtained in Li-rich cathode oxides which has a three-dimensional disordered cation framework.[80] The research suggested that the different structure dimensionality in Li-rich cathode oxides should be responsible for their diverse oxygen lattice structure response to l-OR. For some nano anode materials, such as metal oxides, NPDF was employed to study their structure–property relation. For instance, Liu *et al.* demonstrated that powder x-ray diffraction and NPDF can be used to obtain accurate atomistic structure and morphology of anatase TiO_2 nanocrystals based on differential evolution refinements using Debye scattering equation calculations.[81] In the meantime, they also quantitatively analyzed the stacking disorder and interlayered structure of δ-MnO_2 via NPDF.[82]

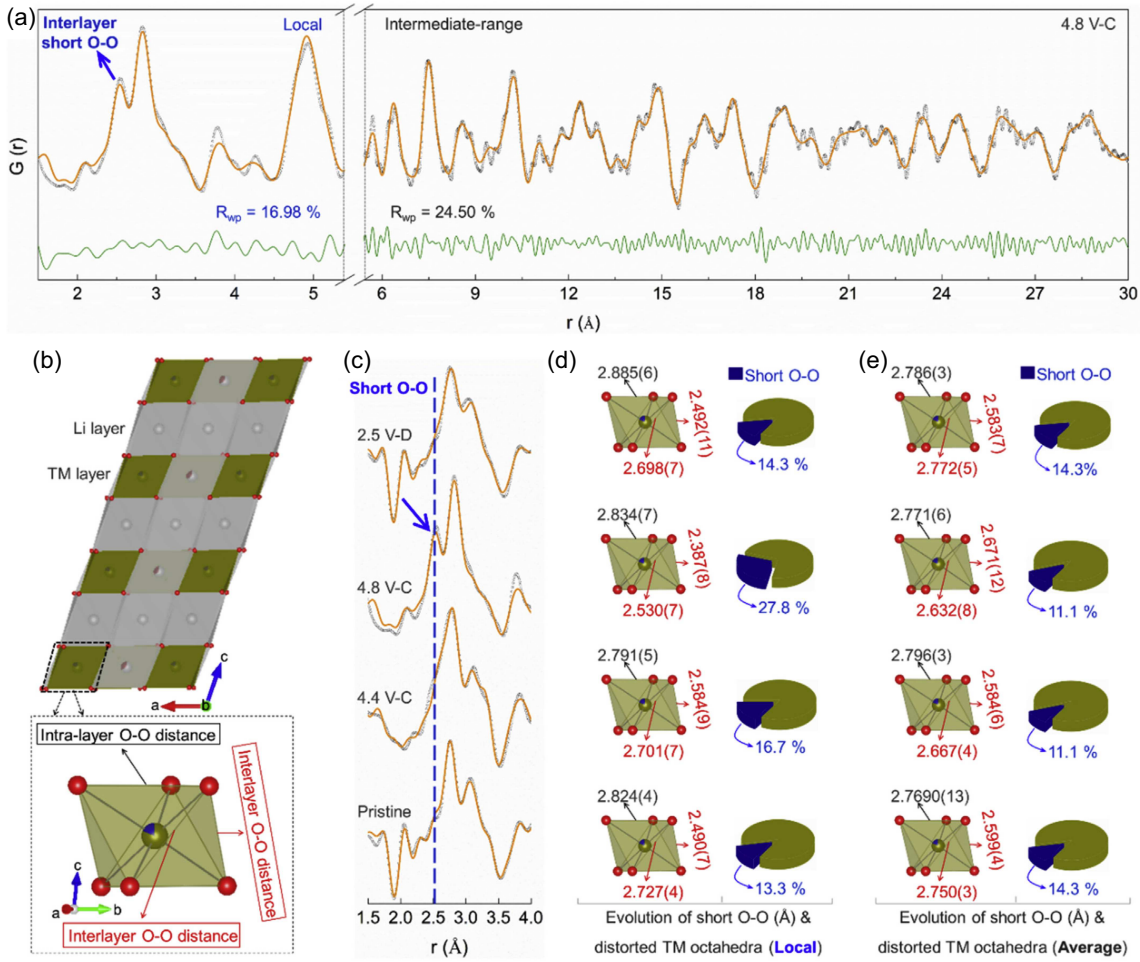


Fig. 3. (a) Refinement results using local (left panel) and intermediate-range (right panel) neutron PDF at 4.8 V charged state. (b) Schematic of interlayer and intralayer O–O distance in the TM octahedra. (c) Comparison of the *ex situ* NPDF results of LMR-NMC collected at different charge-discharged states. (d), (e) The variation in percentage of short O–O pairs and distorted TMO_6 octahedra in local (d) and average (e) structures during the first cycle. Reproduced with permission.[79] Copyright 2019, Elsevier.

3.3. Small angel neutron scattering

As a complementary scattering technique to NPD and NPDF, SANS detects the structure of materials at larger length scales, from 1 nm to micron sizes. The SANS tool is usually used to provide the size and shape information of materials on the nanometer scale. Within the approximation of SANS, Q simplifies to $Q = 2\pi\theta/\lambda$. Usually, the SANS Q range is typically from 0.001 $Å^{-1}$ to 0.3 $Å^{-1}$, below this range is often called ultra-small-angle scattering and above this range is well known as wide-angle scattering. Of course, no hard boundary is defined between them. A suitable model is critical to obtain the accurate structure information during fitting the SANS spectra. Although the particle shape and size (or size distribution) are often the desired structural information, they are not easily solely extracted from the polydisperse systems. Since the spherical object model has the simplest analytical formula for the form factor among all the geometry objects, such as cylinder model, disk model, etc., it has been widely used in SANS data analysis.

The characteristics of SANS make it a powerful method to understand the complicated electrochemical processes, including the formation of SEI, microstructure evolution, etc., occurring in rechargeable LIBs. The SEI in Li-ion battery system has a great importance effect on the electrochemical performance and safety. Based on the advanced SANS technique, several researches have been conducted to explore the formation mechanism, chemical nature as well as the morphology and size evolution process of SEI in LIBs. By employing the time-resolved *in situ* SANS tool, Bridges *et al.* reported a work aiming at presenting a better understand for the electrochemical processes occurring on ordered mesoporous hard carbon anode upon the electrochemical cycling (Fig. 4(a)).[83] They observed the formation and evolution of SEI via introducing electrolytes which contain mixtures of deuterated (^{2}H) and nondeuterated (^{1}H) carbonates. More specifically, SANS detected the formation of an SEI layer in the pores of the carbon framework and the change in the chemical composition of the SEI layer during the discharging process (Fig. 4(a)).[83] Considering that the SEI is a complicated system, Sacci and coworkers simplified it by chemically lithiating graphite (C), increasing its surface area, and then exposing it into organic

solvent to construct the SEI layer.[87] SANS data indicated that the SEI fills the 20–30 nm sized pores and the SEI is larger on LiC_6 than on LiC_{12}. A rough Li–graphite surface, which is ascribed to the 1–2 nm sized domains SEI structure, was observed by further analyzing the SANS data.[87] The research also revealed that the formed SEI would hinder solvent molecules from diffusing into the pore surfaces because of the existence of unfilled nanoscale spaces in the reacted model compound. The silicon/graphite (Si/C) compound, which possesses a high specific capacity, has been considered as the candidate anode for high-energy-density LIBs. Unfortunately, upon the de-/lithiation process, there is always a large volume and structure change in the Si/C anode, which is closely associated with the formation of porous silicon structure and detrimental side reactions at the Si/electrolyte interface. Paul *et al.* used *ex situ* SANS measurements to quantify these morphological and structure changes. They suggested that the formed SEI products could fill the porous nanostructures and there is a nano-porous microstructure with a prominent mean size of 8 nm and a broad size distribution ranging up to 30 nm in the silicon nanoparticles within the aged Si/C electrodes.[88] Recently, in the research work conducted by Jafta *et al.*, they used *operando* SANS to evaluate the dynamic chemistry in LIBs.[84] An interesting phenomenon was revealed that both the viscosity of the electrolyte and size of the surface pores have obvious influence on the formation mechanism of SEI layer upon cycling (Fig. 4(b).[84] The Li-rich salts formed at much higher potentials in the micropores of high-viscosity electrolyte, while the Li-rich reduction products formed quickly before giving way to carbonaceous products on the mesopore surface.

Owing to the mechanical flexibility and thermal stability, high-molecular-weight polymers combined with Li salts have attracted much attention as the solid-state electrolytes. However, their relatively low ionic conductivity at room temperature and low lithium ion transport number limit the performance of the cell containing high power density. Thus, the revelation of their structure–property relation is significant for improving their performance. Bergfelt *et al.* reported a series of deuterated tri-block copolymers and used SANS to study their bulk morphology at various temperatures, confirming the lack of microphase separation in the electrolytes.[89] SANS data showed that the peak evolution, in intensity and q-position, was fully reversible with temperature, which excluded any reordering of the copolymer toward any more thermodynamically stable morphology.[89] In the meantime, *operando* SANS was used to investigate the suitability of Li-metal batteries based on solid single-ion diblock copolymer electrolyte as safe batteries using lithium metal anodes.[90] In addition to the polymer electrolytes, SANS also advanced the structure understanding of NASICON glass-ceramics and aqueous electrolytes. Specifically, based on the SANS data, Vizgalov *et al.* demonstrated that the improved ionic conductivity of Y-doped glasses originated from its sudden crystalline upon heat treatment and formation of uniform $Li_{1+x}Al_xGe_{2-x}(PO_4)_3$ ceramics (Fig. 4(c)),[85] while Borodin *et al.* evaluated the ion solvation and transport behaviors in aqueous electrolytes containing bis(trifluoromethanesulfonyl)imide.[91]

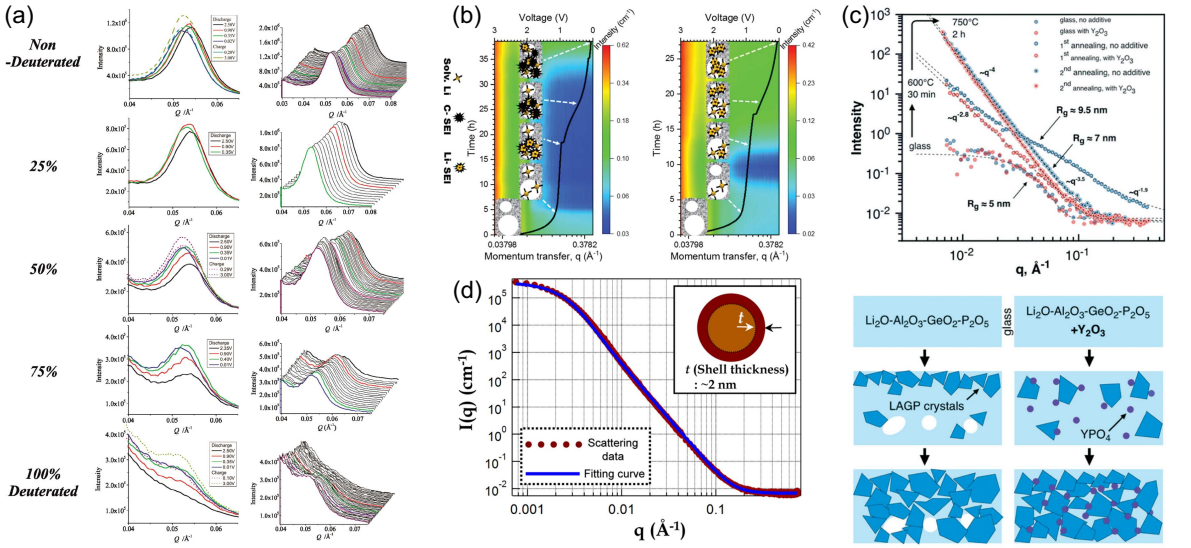


Fig. 4. (a) The *in situ* SANS data for cycling of half-cells containing ordered mesoporous hard carbon cathodes,[7] Li anodes, and 1.0 M $LiPF_6$/EC/DMC electrolyte. Reproduced with permission.[83] Copyright 2012, American Chemical Society. (b) The SANS intensity as a function of the scattering vector for the 1 M LiTFSI/PC (left panel) and the 4 M LiTFSI/PC (right panel) electrolyte systems. Reproduced with permission.[84] Copyright 2019, The Royal Society of Chemistry. (c) SANS curves for the Y-containing and Y-free glass-ceramics at different stages of the crystallization process (top panel) as well as the schematics of the suggested crystallization pattern (down panel). Reproduced with permission.[85] Copyright 2018, The Royal Society of Chemistry. (d) Coherent SANS intensity profile, good agreement with the experimentally obtained scattering data (red dots) was observed when a model function (blue line) based on polydisperse spheres with a shell was applied for data fitting. Reproduced with permission.[86] Copyright 2018, American Chemical Society.

SANS has also been widely used for the nanostructure as well as surface structure research of electrode materials. Chung *et al.* directly demonstrated that the antisite exchange defects are distributed in a highly anisotropic manner near the surfaces of $LiFePO_4$ crystals by combing SANS and scanning transmission electron microscopy (Fig. 4(d)).[86] The research provided guidance for retarding the degradation of lithium mobility through the surface in olivine phosphates.[86] For Li-rich cathode materials, He *et al.* designed a carbonaceous compound on their surface to improve the overall electrochemical performance and, using SANS data, confirmed the presence of carbonaceous compounds in the surface composition.[92] In addition, by employing the SANS technique, Ferguson *et al.* cleared the reason why Sn–Co–C alloys only prepared by the sputter deposited method can achieve the expected capacity.[93] It was found that there are small grain sizes, on the order of 10 Å, in the sputtered samples, while much larger grain sizes were obtained for samples prepared by other methods.[93] The results highlighted the importance of nanostructure in achieving the high capacity for alloy–C composite electrodes. Self-organized nanotube arrays, as an effective strategy, are usually used to modify the performance of nano anode materials like TiO_2. In the research work conducted by Paul *et al.*, a time-of-flight grazing-incidence SANS technique was used to determine the morphology of the nanotube arrays because of the large probed volume.[94] The data showed the different signatures of a prominent lateral correlation of the TiO_2 nanotubes of about 94 nm with a nanotube radius of about 46 nm.[94] This accurate and effective characterization of SANS is significant for the further development of more useful electrode morphologies.

3.4. Neutron reflection

NR, as a powerful tool, is widely used to probe the structure and kinetics at and close to the interfaces of materials. Within certain constraints, the NR measurement can obtain the scattering characteristics beneath a surface by detecting the reflected intensity as a function of angle. The total reflection would occur above a critical angle (representing Q), and below which, each layer interface would produce an oscillating reflected amplitude with period $\Delta Q = 2\pi/T$, where T is the thickness of the layer. Usually, in a NR experiment, the variation of sample composition within the depth of the sample is the desired information, which can be extracted from the scattering-length density profile. The scattering-length density is the sum over the number density of each isotope at a certain depth, times its bound coherent neutron scattering length. Similar to the SANS data analysis, establishing a suitable fitting model for the measured NR signal is also of great significance to obtain the accurate results.

As a complementary and similar technique to SANS, NR has also been demonstrated highly effective for investigating the *in situ* growth and evolution of SEI layer in LIBs. Specifically, NR not only can detect the porosity, structure, and chemical composition of the SEI, but also is sensitive to its structure and composition gradients as well as the thickness.[95,99] Owejan *et al.* designed an *in situ* NR measurement of the SEI layer as a function of the potential in a working lithium half-cell.[95] NR data indicated that, after a series of potentiostatic holds, the SEI thickness of 4.0–4.5 nm for 10–20 CV cycles grew to 8.9 nm (Fig. 5(a)). It was found that, after a rapid increase of the SEI thickness, its growth will become slow even at the lowest potentials examined due to the passivating nature. It should be noted that there are no obvious gradients of the SEI layer based on the scattering-length density profile in this research, which is contrary to the proposed structures in the literature. Meanwhile, NR combined with *in situ* experiment method was performed to study the SEI formation on other electrode materials, such as crystalline carbon,[100] silicon,[101] etc.[102] For instance, in the research work conducted by Steinhauer *et al.*, a lithium-rich adsorption layer was found to be already present on the carbon sample surface at the open circuit voltage and the first decomposition products started to deposit close to this potential.[100] Based on the NR data, a maximum SEI thickness of 192 Å at the lower cutoff potential was observed, which slightly decreased during the positive potential scan. In addition, NR played an important role in understanding the new solid–liquid electrolyte interphase in the hybrid battery system which combines both solid and liquid electrolytes. Using *in situ* NR technique, Weiss *et al.* studied the formation of interphase between the solid electrolyte lithium phosphorous oxide nitride ($Li_xPO_yN_z$, LiPON) and various liquid electrolytes.[103] They demonstrated that the interphase is composed by two layers, one is a nonconducting layer directly in contact with LiPON and the other is a lithium-rich outer layer. The eventual thickness of the interphase is about 20 nm after an initially fast growth and slow growth in the late stage.[103] Overall, the above research work highlights the ability of *in situ/operando* NR method in exploring the "live" composition/decomposition process of SEI layer under cell operation.

Another important application of NR technique is to study the electrochemical reaction mechanisms, such as the Li permeation,[104–106] lithium storage,[107,108] lithium transport,[96] etc., of LIBs. Considering the characteristic of NR measurements, a special ultrathin/film electrode or cell setup is usually essential. Amorphous silicon has been considered as the most promising candidate anode due to its ultrahigh theoretical specific capacity of almost 4000 mA·h/g. Pre-lithiation of silicon is an effective strategy to modify the cycle performance of the silicon anode. Understanding the Li permeation behavior through amorphous Li_xSi layers is

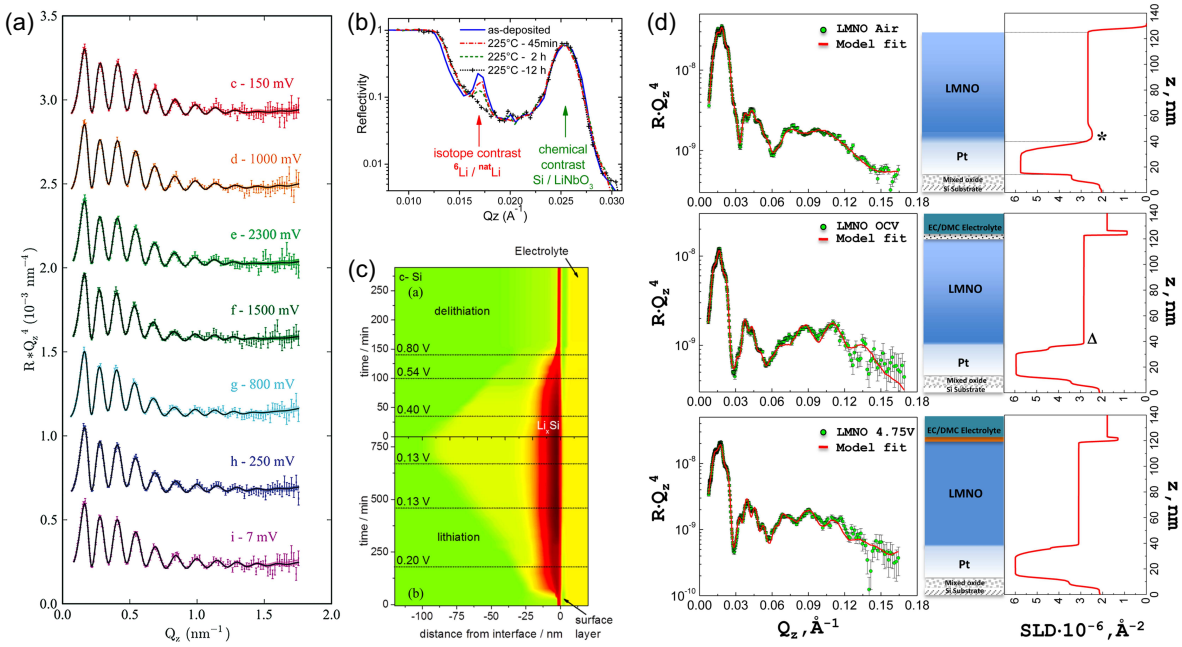


Fig. 5. (a) Neutron reflectivity (expressed as $R \times Q^4$) vs. Q for the sample measured during holds at the corresponding potentials. Reproduced with permission.[95] Copyright 2012, American Chemical Society. (b) NR patterns of the multilayer system at various states. Reproduced with permission.[96] Copyright 2013, American Chemical Society. (c) SLD profiles of the second lithiation and the second delithiation as a function of time and distance from the interface. Reproduced with permission.[97] Copyright 2016, American Chemical Society. (d) Neutron reflectivity profiles collected *in situ* for the $LiMn_{1.5}Ni_{0.5}O_4$ film (top left) in air, (middle left) at the open circuit voltage, and (bottom left) charged to 4.75 V, the corresponding SLD plots represent the film thickness (top right, middle right, bottom right) and the schematics in the middle represent the layers formed from the silicon substrate out. Reproduced with permission.[98] Copyright 2014, American Chemical Society.

significant for the pre-lithiation engineering. For the measurements of Li permeation, a multilayer structure consisting of five [Si/^{nat}LiNbO$_3$/Si/^{6}LiNbO$_3$] units which was produced by ion beam sputtering was designed in the research conducted by Erwin and co-workers (Fig. 5(b)).[104] Based on the variation of the Bragg peaks detected in the NR patterns under different conditions, the Li permeability (solubility × diffusivity) can be derived.[104] In the meantime, they also used (*operando*) NR technique to study the lithium transport through nanosized amorphous silicon layers as well as the volume expansion during lithiation of amorphous silicon thin film electrodes.[96,109] For example, a lithium permeability of $P = (1.28 \pm 0.25) \times 10^{-16}$ cm^2/s was observed based on the decrease of the ^{6}Li/^{7}Li Bragg peak as a function of annealing time at 225 °C. NR can also be used to study the kinetics of lithiation and de-lithiation of silicon because of the strong scattering contrast between silicon and lithium.[97,107] By employing *operando* NR, Seidlhofer *et al.* revealed that, during the first charge step, the lithiation of silicon starts with the formation of a lithium enrichment zone.[97] It was also found that there is no difference of the high lithiation zone thickness between the first two cycles, whereas the thickness of the less lithiated zone is larger for the second lithiation (Fig. 5(c)). Jerliu *et al.* using *in situ* NR experiments studied the capacity loss mechanism of amorphous silicon thin film electrodes during the first ten cycles.[108] By analyzing the neutron scattering length density and film thickness, it was reported that the capacity loss of the silicon anode is due to irreversible storage of lithium in the electrode.

As is well known, the interaction between the electrode and electrolyte has a significant effect on the electrochemical performance of LIBs. Thus, it is important to investigate their surface/interface structure evolution. By employing *in situ* NR, Browning *et al.* probed the thickness and scattering length density profile of the electrode–electrolyte interface for the high-voltage cathode $LiMn_{1.5}Ni_{0.5}O_4$ at the open circuit voltage and fully delithiated states (Fig. 5(d)).[98] NR data indicated that there is a formation of thin 3.3 nm Li-rich interface because of the ordering of the electrolyte on the cathode surface. Furthermore, they found an increase in the scattering length density of the new layer which indicated that the composition of the interface changes with charging process. For the dynamic behavior of the interface between $LiCoO_2$ and organic electrolyte, using *in situ* NR tool, Minato *et al.* found that the composition and thickness of the interface would change during the Li-ion extraction/insertion process.[110] Specifically, the thickness of the interface layer would increase and decrease upon the Li-ion extraction and insertion, respectively.[110] In addition, NR was employed to investigate the surface structure evolution of $Li_4Ti_5O_{12}$ electrode upon the electrochemical reaction process and the surface modification mechanism of lithium-rich layered rock-salt oxide cathodes.[111,112]

3.5. Neutron imaging

Neutron imaging, usually also called neutron radiography, is a nondestructive technique which can visually reveal the bulk structure information of materials. The basic principle of NI technique is to use the attenuation change of neutron beam in the intensity when it passes through the sample, observing the perspective image of the measured object. With the improvement of the spatial and temporal resolution of the detectors as well as the development of various computational methods, some advanced NI techniques, such as Bragg-edge imaging, three-dimensional tomography, phase-contrast imaging, etc., are allowed. Take Bragg-edge imaging as an example, its spatial resolution is higher than the traditional NI method though there are some challenges for its experiment measurements and data analysis. As a complementary technique to NPD, NPDF, SANS, and NR, NI is often widely performed to detect the macroscopic dynamic and chemical information within LIBs. In addition, similar to NPD, NI, especially for its *in situ* measurements, is also usually used for the research of commercial batteries.

Understanding the electrochemical behavior of lithium ions, including the Li-ion transport, Li-ion spatial distribution, and Li-ion concentration evolution, upon the cycling process is of great significance for the optimization of the overall battery performance. Due to the strong neutron attenuation of ^{6}Li as compared to ^{7}Li, NI has been considered as a powerful and direct tool to study the above fundamental scientific questions correlated with lithium. Using NI, Owejan conducted a continuous measurement of through-plane Li-ion distribution in an electrochemical cell with the composite graphite as the negative electrode.[117] The measured NI results indicated that the lithium distribution within the graphite electrode is presented as a function of the state of charge. Zhang *et al.* studied the Li-ion spatial distribution within V_2O_5 electrode in a small coin cell by neutron computed tomography.[118] They found that the Li-ion spatial distribution is inhomogeneous in the electrode, and a relatively higher current rate would result in a more non-uniform Li distribution after the insertion process of lithium ions. This phenomenon indicated that the Li-ion diffusion in the electrode is usually dependent on the cycling rate upon the lithiation process.[118] In the meantime, Zhang and co-workers probed the spatial distributions of Li ions in electrochemically delithiated Li–Mg alloy electrodes and observed the Li concentration profiles along the thickness direction.[119] For the Li-ion concentration evolution, Siegel *et al.*, using the *in situ* NI technique, quantified it at various states of charge in a $LiFePO_4$ pouch cell battery (Fig. 6(a)).[113] In addition, NI combined with *in situ* experiment method was used to track the lithiation and delithiation processes in the electrode during cycling. For instance, by employing *in situ* NI, Nie *et al.* found that the lithiation/delithiation processes are qualitatively consistent with calculations of the Li^+ concentration and discharge profiles of the cell.[120] More specifically, a uniform lithiation of the $LiCoO_2$ electrode upon the discharging process as well as the delithiation that started near the $Li_4Ti_5O_{12}$ current collector in the thicker $Li_4Ti_5O_{12}$/$LiCoO_2$ battery was observed.

NI also played an important role in understanding the manufacturing process, such as the filling of liquid electrolyte, of Li-ion battery cells.[114] Since the electrolyte filling during the cell production process will directly determine the electrochemical properties as well as the safety performance of the cell, providing an insight into the filling process is significant. Using NI, Knoche and co-workers visualized the soaking behavior of electrolyte liquid within the battery during the filling and wetting process (Fig. 6(b)).[114] According to their research, to prevent the gas entrapments, it is critical to ensure a directional flow of electrolyte liquid within the electrode assembly. During the filling process, another important aspect that should be ensured is that the gas trapped between or within the porous media is not hindered in leaving the electrode-separator-assembly (Fig. 6(b)). The findings in this work indicated that a well-engineered filling process can reduce the wetting time, thus leading to cost saving in cell manufacturing and high-performance batteries.[114] The gas release upon cycling in LIBs can not only degrade the cell performance but also cause potential safety hazard. Therefore, understanding the gas evolution mechanism and its origin is also of great importance. Early research work has demonstrated that NI is a very suitable tool to *operando* observe the gas evolution in battery cells.[121] By comparing the evolved gas volume of different anode/cathode, it was found that $LiNi_{0.5}Mn_{1.5}O_4$/graphite batteries contain the highest amount of gas possibly due to the dissolution of Mn ions.[121] The similar conclusion was also obtained in the research work conducted by Starke *et al.*[122] Specifically, NI results showed that in $LiFe_xMn_{1-x}PO_4$/graphite cells, approximately 30% more gas is generated compared with that in $LiFePO_4$/graphite and the stronger gas evolution is closely correlated with the presence of Mn ions.[122] The important results obtained from NI data highlight the necessity of hindering the dissolution of Mn ions in active materials to reduce the gas evolution.

As mentioned at the start of this section, Bragg-edge imaging, due to its high resolution, has attracted wide attention in the battery research. The Bragg edges originated from the diffraction of the neutrons by crystals are usually obtained in the transmission spectra as a function of neutron wavelength by the pulsed neutron transmission method.[115] The lattice spacing and the surface density of the corresponding crystalline material can be reflected from the position of the

Bragg edge and the depth of the edge, respectively.[115] In this imaging method, the results of surface density are not influenced by neutron absorption as well as neutron scattering. Through the Bragg edges analysis, Kino *et al.* gained the two-dimensional imaging of electrodes during the charging and discharging process (Fig. 6(c)).[115] Meanwhile, Kamiyama *et al.*, using Bragg-edge imaging, studied the structural change of carbon anode upon the charging process in a $LiFePO_4$/graphite lamination-type full cell.[123] During this measurement, the graphite (002) Bragg-edge was focused, and recognized on the neutron transmission spectra. It was revealed that the Bragg-edge shifted and broadened continuously during the overall charging process, and the edge was consistent with the existence of multiple graphite structural stages. At different charging levels, the distributed layer spacing images were observed, indicating the inhomogeneous fluctuation on the lattice plane of LIBs.[123] Also, in the research work conducted by Senyshyn and co-workers, the spatial evolution of selected Bragg reflections for $LiCoO_2$ cathode, graphite, and lithium intercalated graphite was observed to evaluate the lithium distribution in 18650-type LIBs (Fig. 6(d)).[116] By employing the computed neutron tomography, a homogeneous lithium distribution in the battery cell was confirmed.[116]

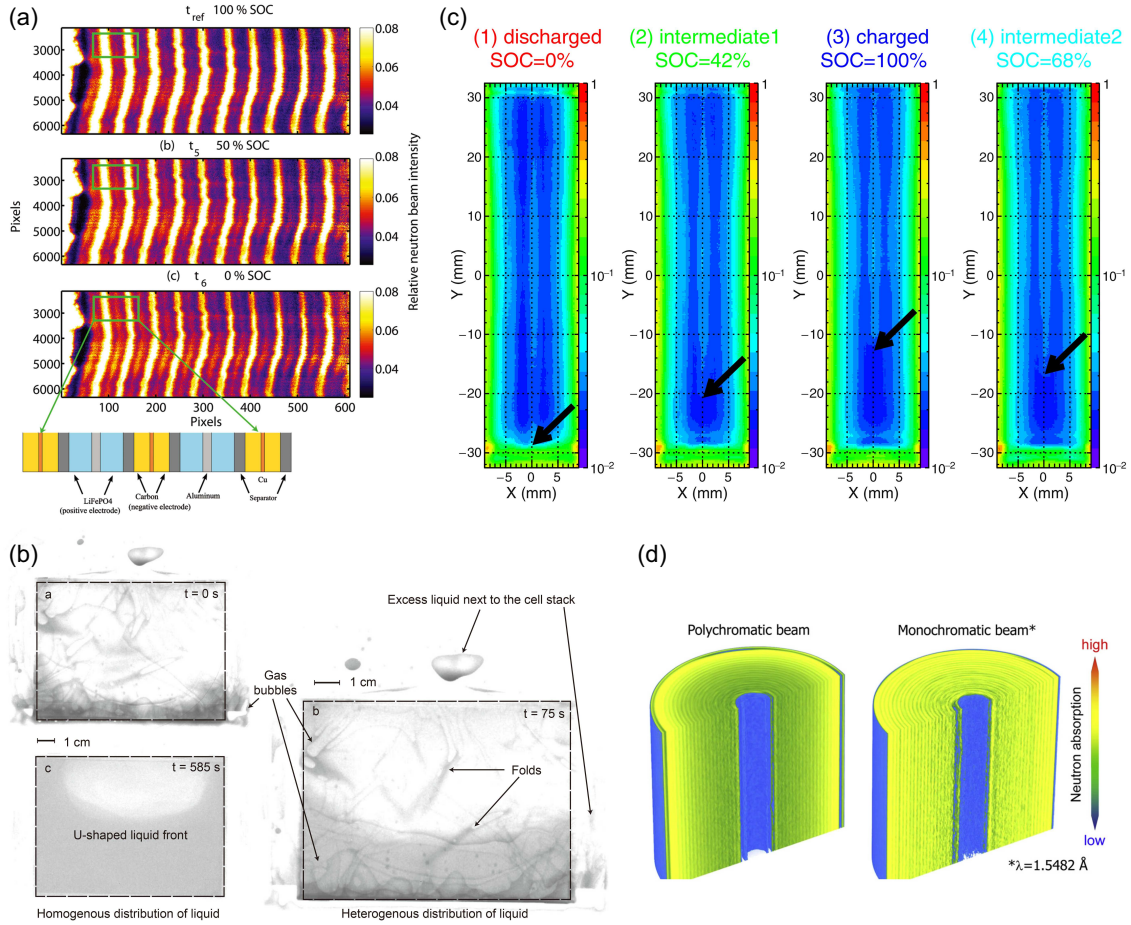


Fig. 6. (a) Images from the cycling profile corresponding to time t_{ref}, t_5, and t_6. Reproduced with permission.[113] Copyright 2011, The Electrochemical Society. (b) Calibrated images of one cell immediately, 75 s, and 585 s after injection of the liquid, the position of the cell stack is shown by the broken lines, and the brightness and contrast are adjusted for ease of viewing. Reproduced with permission.[114] Copyright 2016, Elsevier. (c) Transmission images of the four charge states in the neutron wavelength range from 0.1 nm to 0.8 nm. Reproduced with permission.[115] Copyright 2016, Elsevier. (d) 3D visualization of the commercial 18650 Li-ion cell (discharged state), reconstructed from neutron radiography based on data acquired using a "white" neutron beam (left) and monochromatic neutrons (right). Reproduced with permission.[116] Copyright 2016, Elsevier.

3.6. Neutron depth profile

Differ from the above neutron-based characterization techniques, NDP is a quantitative analytical tool which is commonly used to detect the elements that exhibit a high probability of absorbing neutrons as a function of depth. Based on this characteristic, NDP technique is allowed to directly probe the lithium nuclei by the capture reaction of neutrons with the ^{6}Li isotope to form an α -particle (^{4}He) and a triton (^{3}H) according to $^6\text{Li} + \text{n} \rightarrow {}^3\text{H}$ (2727.9 keV) $+{}^4\text{He}$ (2055.5 keV). In this capture reaction, the produced particles, i.e., ^{4}He and ^{3}H , would lose part of their kinetic energy when passing through the sample before reaching the detector that is housed in a high-vacuum chamber. Thus, the depth of the capture reaction

can be reconstructed by measuring the residual energies of the emitted ^{4}He and ^{3}H particles. Meanwhile, through comparing the number and residual energies of the particles against a standard sample, the concentration distribution versus depth from the surface can also be calculated. Normally, for a well-defined homogeneous layer, the spatial resolution of NDP is on the order of tens of nano-meters.

The above working principle of NDP determined that it is a perfect tool for the analysis of the lithium-ion diffusion, concentration distribution, and reaction rates as a function of depth, which opens a large range of opportunities including the research of alloying reactions, Li metal plating/stripping, and (de) intercalation mechanisms in LIBs.[124,125,128–133] For instance, by employing *operando* NDP, Zhang *et al.* directly observed the Li-ion concentration profiles in the $LiFePO_4$ electrode and revealed that the rate-limiting step is dependent not only on the morphology of the electrodes but also on the cycling rate itself.[128] Liu *et al.*, using *in situ* NDP, studied the onset of lithiation in a high-capacity Sn anode, specifically, Li atoms first enriched on the surface and then propagated into the bulk of the Sn anode.[124] The decreased coulombic efficiency upon delithiation process was ascribed to the removal of Li near the surface which originated from the trapped Li within the intermetallic material (Fig. 7(a)). Meanwhile, Lv and co-workers investigated the lithium plating and stripping mechanism in detail through *operando* NDP.[125] It was revealed that the evolution of the lithium-metal-density-profile is closely correlated with the current density, electrolyte composition, and cycling history (Fig. 7(b)). *Operando* NDP also indicated that the majority of the Li uptake in Cu is reversible, almost penetrating the 10 μm thick Cu current collector.[125] In addition, NDP provided insights into the lithium concentration in other negative electrode materials. Specifically, through NDP technique, Ceccio *et al.* obtained the diffusion coefficient of Li into the porous carbon and evaluated the porosity parameters of the porous carbon,[129] while Wetjen *et al.* monitored the evolution of lithium concentration profiles across the thickness of porous silicon-graphite electrodes during the first cycle, observing the depth- and quantity-resolved SEI formation, and changes of the total lithium content as a function of the (de)lithiation states.[130]

For the degradation or aging mechanism research of LIBs, NDP also played an important role. In the research work conducted by Nagpure *et al.*, NDP was applied to study the aging mechanisms of $LiFePO_4$-based lithium-ion batteries that are designed to be aged at different rates to different states of charge.[134] The cycling rate as well as the state of charge has an obvious effect on the Li concentration profile. It was also found that although the Li concentration profile changed along the length of the electrode from the outer edge to the core of the cylindrical cell, it remained constant along the height of the electrode. Other than the above data, lots of quantitative parameters correlated with the lithium concentration profiles for anode and cathode were also provided by NDP.[134]

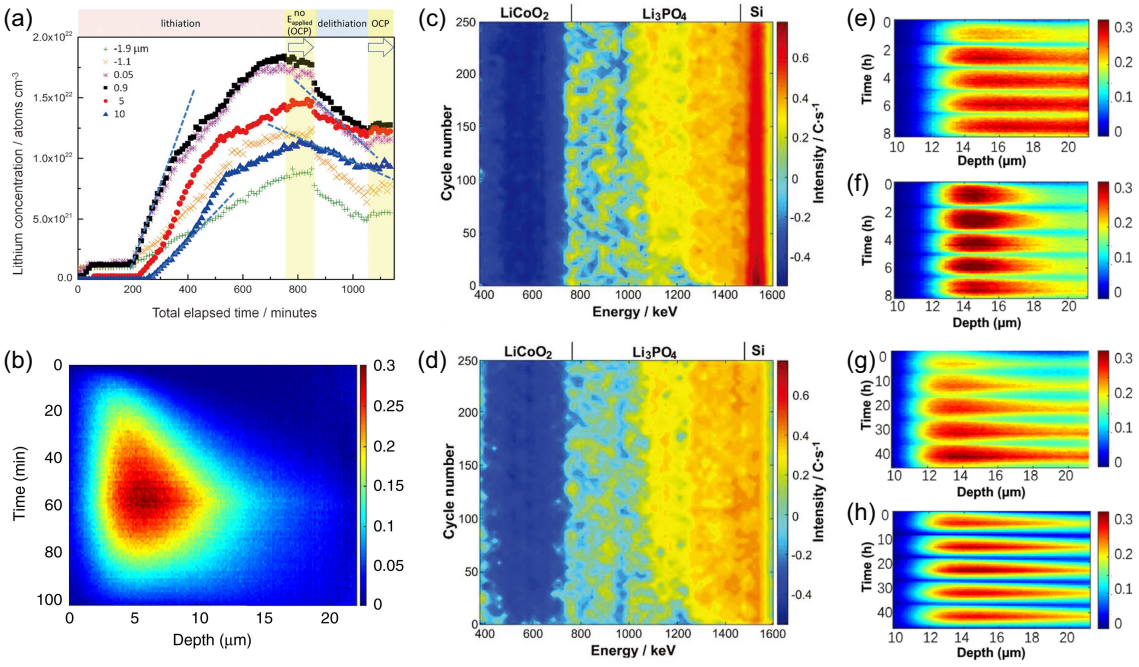


Fig. 7. (a) Lithium concentration at various regions of the battery as a function of lithiation and removal of the applied potential, delithiation and removal of the applied potential. Reproduced with permission.[124] Copyright 2014, Wiley-VCH Verlag GmbH & Co. KGaA. (b) The Li density vs. time from *operando* NDP during the first plating and stripping cycle. Reproduced with permission.[125] Copyright 2018, Nature Publishing Group. Development of the measured NDP spectra as a function of energy for (c) a fully charged and (d) discharged battery upon cycling up to 250 cycles. Reproduced with permission.[126] Copyright 2018, Wiley. Li distribution from *operando* NDP of the (e) Cu/LE/Li batteries and (f) Cu/LE-LNO/Li batteries for five plating/stripping cycles at 1 mA/cm^2, Li distribution from *operando* NDP of the (g) Cu/LE/Li batteries and (h) Cu/LE/Li batteries for five plating/stripping cycles at 0.2 mA/cm^2. Reproduced with permission.[127] Copyright 2019, American Chemical Society.

Due to the essential difference of electrolyte between the classical liquid electrolyte cells and all-solid-state batteries, the aging or degradation mechanisms in all-solid-state batteries are also different. For further understanding of the aging behavior in all-solid-state batteries, by introducing *operando* NDP, Chen *et al.* conducted a research regarding the degradation mechanism of all-solid-state thin film Si–Li_3PO_4–$LiCoO_2$ batteries (Figs. 7(c) and 7(d)).[126] They indicated that the capacity loss in these thin film batteries mainly originated from the lithium immobilization in the solid-state electrolyte, which started to grow at the anode/electrolyte interface during the initial charging. It was concluded that the immobilized Li layer in the electrolyte is induced by silicon penetration from the anode into the solid-state electrolyte and continues to grow at a lower current density upon the subsequent cycling process.[126] In addition, as an effective post mortem analysis tool, in the research work conducted by Wetjen *et al.*, NDP was employed to quantify the amount of lithium-containing electrolyte decomposition products (e.g., SEI), determine their distribution across the electrode thickness, and monitor the active material utilization across the electrode over long cycles.[135]

Solid state electrolytes are promising to replace the traditional liquid electrolytes and work with Li metal safely because of their nonflammable and well mechanical properties. However, the poor contact between the electrodes and solid-state electrolytes as well as the uncontrolled interface dendrite growth limit their practical application. Thus, understanding of the solid-state electrolyte interface mechanism is of great importance for the development of all-solid-state LIBs. In this regard, NDP combined with the *in situ* experiment method shows its ability in studying the interface behaviors and Li dendrite growth phenomenon of solid-state electrolytes. For example, Wang and co-workers, utilizing *in situ* NDP, investigated the interfacial behavior of garnet solid-state electrolyte in contact with metallic Li upon the Li plating/stripping processes.[136] Specifically, in their research work, two types of all-solid-state batteries, one is symmetric Li/garnet/Li cells, the other is asymmetric Li/garnet/carbon-nanotubes cells, are designed to emulate the behaviors of Li metal and Li-free Li metal anodes, respectively. NDP data indicated that there is a limitation for Li-free Li metal anode to form a reliable interfacial contact.[136] In the meantime, by employing time-resolved *operando* NDP, Han *et al.* revealed the origin of the dendrite formation in three types of solid-state electrolytes according to the dynamic evolution of Li concentration profiles.[137] Their research results indicated that there are no apparent changes in the lithium concentration in LiPON, while a direct deposition of Li inside the bulk of $Li_7La_3Zr_2O_{12}$ and amorphous Li_3 PS_4 was observed. The diverse Li deposition behaviors suggested the effect of electronic conductivity of different solid-state electrolytes on the Li dendrite formation.[137] For the carbonate electrolyte gel polymer with $LiNO_3$ addictive, Liu *et al.*, using *operando* NDP, demonstrated its positive role in stabilizing the Li-metal plating.[127] NDP data revealed that when $LiNO_3$ electrolyte additive and the gel polymer approach are used in conjunction, their effects are complementary in increasing the density of the plated Li, reducing the inactive Li species, and reducing the overpotential (Figs. 7(e)–7(h)).[127]

3.7. Quasi-elastic neutron scattering and inelastic neutron scattering

As a direct way to study ion dynamics with neutrons, QENS method is based on the small energy exchanges between the diffusing particles and the scattered neutrons, which usually cause a broadening of the elastic peak. The QENS technique can provide dynamic information on the 0.1–100 nm length scale with characteristic time on the order of 10^{-9}–10^{-12} s, which corresponds to energy transfers on the order of 1 μeV to 1 meV. Differ from the quasi-elastic broadening, INS peaks usually arise at higher energy. Specifically, inelastic peaks are associated with a periodic motion, and the forces controlling this motion are stronger than those that would define a more diffusive motion. Generally, INS technique amounts to "vibrational spectroscopy with neutrons", which is usually employed to study the local structure and vibrational dynamics of materials.

QENS, as a powerful tool, has been widely used to study the Li-ion conductivity behavior and ion dynamics in solid-state electrolytes. Using QENS, Maranas and co-workers studied the polymer dynamics in PEO-based single ion conductors.[138] In this conductor, anions are covalently bonded to a PEO spacer through a comonomer unit and only cations contribute to the conductivity. They conducted the experiment by comparing the effects of changing ion content on the dynamics of the polymer spacer in two cases. Specifically, according to the observed two dynamic classes of spacer atoms, they proposed that the fast [bridge] and slow [anchor] regions in the conductor are spatially segregated. QENS further determined the fraction of bridge and anchor atoms, and estimated their ionic compositions (Figs. 8(a) and 8(b)).[138] Meanwhile, Maranas *et al.* also studied the influence of nanofiller surface chemistry and ion content on the conductivity of nanofilled PEO + $LiClO_4$ solid polymer electrolytes via QENS and other characterization techniques.[141] QENS, which probes mobility as a function of spatial scale, indicated that there are no significant changes in PEO segmental dynamics as a function of surface chemistry. Furthermore, it was found that, in the absence of salt, acidic particles slow PEO dynamics more than neutral particles, which suggested that the PEO chains and the acidic surface sites share a favorable interaction.[141] Other than polymer electrolyte,

QENS was employed to investigate the Li-ion diffusive behavior of garnet-type oxide electrolyte ($Li_{5+x}La_3Zr_xNb_{2-x}O_{12}$) in the research work conducted by Nozaki and co-workers.[142] Combined with μ^+SR results, QENS data shed light on the relationship between σ_{Li} and the number density of mobile Li-ions (n_{Li}) in garnet-type electrolytes.[142] For the Li^+ and BH_4^- dynamics in $LiBH_4/SiO_2$ aerogel composite solid-state electrolytes, QENS measurements found that only a small fraction ($\sim$ 10%) of the ions have high mobilities, whereas most of the $LiBH_4$ shows behavior similar to macrocrystalline material.[143] It was revealed that the modified $LiBH_4$ was formed from interaction with the SiO_2 surface and most probably from reaction with the surface silanol groups.[143]

QENS was applied to study the Li transport in the highly defective amorphous Li_xSi anode materials (Fig. 8(c)).[139] QENS results indicated that the energy of activation of Li self-diffusion in amorphous lithium silicide is 0.20 eV, which is in excellent agreement with the results observed via other methods.[139] Since amorphous Li–Si structures usually have superior Li diffusion than that of their crystalline counterparts, the isolation and stabilization of defective Li–Si structures may improve the utility of Si anodes for Li-ion batteries. In addition, using QENS, Wagemaker *et al.* studied the Li ion position in anatase TiO_2.[144,145] As is well known, the intercalation of Li in TiO_2 anatase will result in a phase separation in a Li-poor and a Li-rich phase. According to the NPD data, they firstly found that there are two distinct positions with a temperature-dependent occupancy within the octahedral interstices in each of the phases. By combining QNES and force field molecular dynamics simulations, they further found that Li is hopping on a picosecond time scale between the two sites in the octahedral interstices.[144] These findings also showed that there is a specific Li arrangement along the crystallographic *a* direction, though without long range order.[144]

The ion mobility and stability of lithium solid conductors play an important role in the electrochemical performance and life time of solid-state LIBs. Accordingly, providing guidance for the performance optimization of solid-state Li-ion conductors is essential. In the research work conducted by Muy *et al.*, INS was used to study the correlation between the lithium ion mobility and lattice dynamics (Fig. 8(d)).[140] By employing a series of lithium ion conductors in the LISICON family derived from Li_3PO_4 as the model compounds, they proposed that the lattice dynamics of the solid-state electrolyte can greatly influence the lithium ion mobility and stability.[140] Specifically, INS data indicated that the lithium vibration frequency or center of lithium phonon density of states for fast lithium conductors is relatively low, and lowering anion

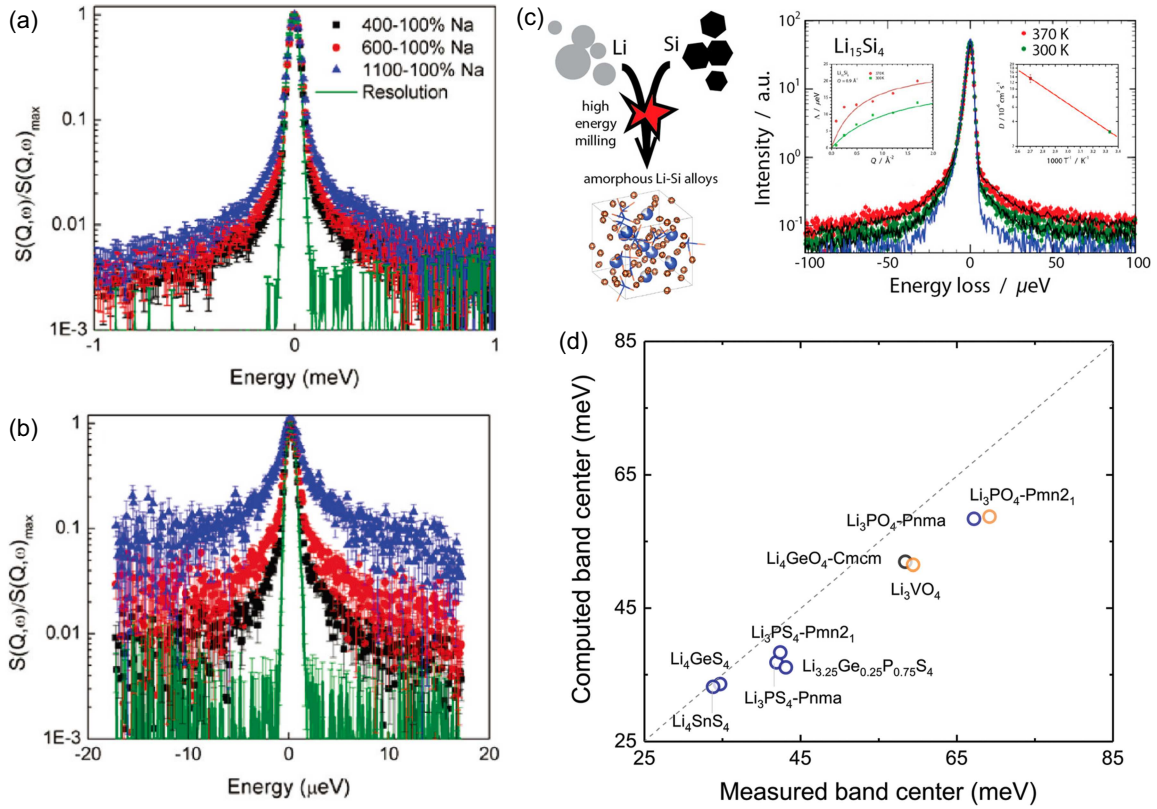


Fig. 8. Frequency domain data from (a) disk chopper spectrometer and (b) high flux backscattering spectrometer for PEO with different ion content at $Q = 1.04$ Å^{-1} and $T = 348$ K. Reproduced with permission.[138] Copyright 2012, American Chemical Society. (c) Observed QENS data for $Li_{15}Si_4$ at 370 K and 300 K, and at momentum transfer 0.9 Å^{-1}. Reproduced with permission.[139] Copyright 2017, American Chemical Society. (d) Comparison between computed and measured total phonon band centers of 7 stoichiometric LISICONs, one substituted LISICON $Li_{3.25}Ge_{0.25}P_{0.75}$ S_4 (chemically similar to $Li_{10}GeP_2S_{12}$) and Li_4GeO_4 (*Cmcm*) at 100 K. Reproduced with permission.[140] Copyright 2018, Royal Society of Chemistry.

phonon densities of states would reduce their stability against electrochemical oxidation. In addition, it was also revealed that olivine-type solid-state electrolytes with low lithium band centers but high anion band centers are promising lithium ion conductors which can achieve both high ion conductivity and good stability against electrochemical oxidation (Fig. 8(d)). For the glass-type superionic, INS was performed to investigate the evolution of Boson peak with the Li-salt concentration.[146] In the $x\mathrm{Li_2SO_4}\cdot(1-x)\mathrm{LiPO_3}$ ($x=0.05$ and 0.3) superionic glasses, it was found that the Boson peak associated with the $x=0.3$ sample would be enhanced and broadened to the high energy side of the peak compared with that of the $x=0.05$ sample, which suggested that the amount of the Li-salt has an obvious effect on the dynamics of the underlying structural framework.[146] Using INS measurements and molecular dynamics simulations, Singh *et al.* studied the phonon dynamics of β-eucryptite.[147] The Li diffusion in β-eucryptite can be observed according to the disappearance of Li-related peaks in the experimental and calculated phonon spectra. They proposed that the presence of defects can enhance Li-ion diffusion as well as lower the temperature for Li-ion diffusion.[147] The above research work based on INS technique highlights the new strategies in controlling lattice dynamics to improve the ion conductivity of lithium ion conductors.

Furthermore, INS was used to study the surface phonons of electrode materials. For instance, by combining INS and first-principles *ab initio* simulations, Benedek and co-workers demonstrated that the structure of the surface of active materials differs from the interior of the particles.[148] In this research, $\mathrm{LiFePO_4}$ with/without carbon coating were selected as the model system, they found that the carbon coating would affect the Li–O bonding on the (010) $\mathrm{LiFePO_4}$ surface relative to the bulk.[148] These findings shed light on the relationship between the vibrations of atoms at the surface and electrochemical behaviors, such as lithium ion transport, charge transfer, and surface reactivity, of the active materials. Xie *et al.*, using theoretical calculations and INS experiments, revealed the relation between the surface structure and Li-ion storage capacities of the functionalized two-dimensional transition-metal carbides or MXenes.[149] They suggested that the Li-ion storage capacities are strongly dependent on the nature of the surface functional groups, with oxygen groups exhibiting the highest theoretical Li-ion storage capacities.[149] For the Li-storage mechanism in carbon-based anodes, Papanek and co-workers using incoherent INS measurements and other characterization techniques found that the structural motif of disordered carbons is a planar graphene fragment, with edge carbons terminated by single hydrogen atoms, and random stacking between fragments.[150] Their research results are consistent with two reported mechanisms for Li capacity, one is partial charge transfer from Li to the carbons, the other is correlated with the C–Li bonding.[150]

4. Design of the *in-situ/operando* neutron-based characterization

Understanding the electrochemical reaction mechanisms, the atomic structure evolution as well as the structure-/dynamic-function relations of LIBs is of great importance for making breakthroughs in their overall electrochemical performance, and fundamental to these is the study of battery materials during operation. Thus, *in situ* and even *operando* studies are commonplace and also essential in Li-ion battery research. As mentioned above, due to the high penetrability, neutron-based techniques are ideal for *in situ/operando* researches. Usually, the commercial cells or pouch cells cannot be directly applied in the *in situ* neutron-based characterization, and the battery component isotopic composition as well as the geometry of the cells needs to be specially designed to obtain the satisfactory results. For instance, due to the large incoherent neutron scattering cross section of hydrogen, deuterated electrolytes and special fluorinated separators are commonly used to reduce the incoherent background. In addition, limited by the difficulty of data analysis or the time-resolution of characterization tools, at present, the reported *in situ/operando* neutron scattering methods mainly focused on NPD, SANS, NR, NI, and NDP techniques.

4.1. The *in situ* NPD

Since the early research of a custom-made cell for *in situ* NPD was reported,[152] several cell designs, including coin-type cells, cylindrical-type cells, and pouch-type cells, have been developed to meet the requirements of *in situ/operando* NPD measurements. In the research works conducted by Rosciano *et al.* and Godbole *et al.*, polyetheretherketone polymer and aluminum/titanium were used, respectively, to manufacture the compartment, where active electrode materials were encased, of *in situ* coin-type cells.[153,154] Due to the strong background and overlap of the diffraction peaks of the compartment with those of electrochemical active materials, it is not easy to observe the accurate refinement structure information during cell operation. To solve this problem, Bianchini *et al.* introduced the Ti–Zr alloy, which is transparent to neutron, in the *in situ* coin-type cell, and achieved the structural refinements of diffraction patterns upon the cell operation process.[155] Commonly, a large amount of active materials is essential to obtain a diffraction pattern with sufficient intensity in a reasonable measurement time in NPD experiment. Unfortunately, the large amount of loose powder in the *in situ* coin-type cell is not favorable for the electrochemical

performance, such as cycle life, rate capability, etc., which directly restricts the *in situ/operando* battery research upon long cycles or at high operation rates. Cylindrical-type cells and pouch-type cells are suitable design strategies to overcome these challenges. Specifically, Sharma *et al.* designed an *in situ* 18650-type cell by rolling the positive electrode, separators, and lithium foil inside a vanadium tube,[156] while Roberts *et al.* and Brant *et al.* modified the design by closing a cylindrical cell (quartz or aluminum casing) with Swagelok-type metallic current collectors achieving high-rate cycling of the cell.[157,158] Furthermore, as shown in Fig. 9(a), Vitoux *et al.* optimized the *in situ* cylindrical cell to achieve the long-life cycling and low absorption from the inactive components, including electrolyte, separator, and casing, located in the beam path.[151] Also, for the *in situ* pouch-type cell, it has been attracted wide attention because of its simple construction process and flexibility in the choice of cell components.[159,160] Similar to the manufacture process of their commercial products, the cathode, anode, and separator are stacked and wrapped in a propylene-coated aluminum pouch, and then the electrolyte is injected in it, followed by a heat-sealed step. In this system design, the anisotropic absorption of neutron induced by the non-radial geometry of the pouch cell could affect the observation of the final structural information. It has been demonstrated that the special geometry design of the sample or cell could effectively minimize such detrimental influence.[159] In addition, other type electrochemical cells for *in situ* NPD were also reported. For example, Vadlamani *et al.* designed a special *in situ* cell using single crystal (100) Si sheets as the casing material as well as the planar cell configuration, providing an improved signal-to-noise ratio compared with other casing materials.[161]

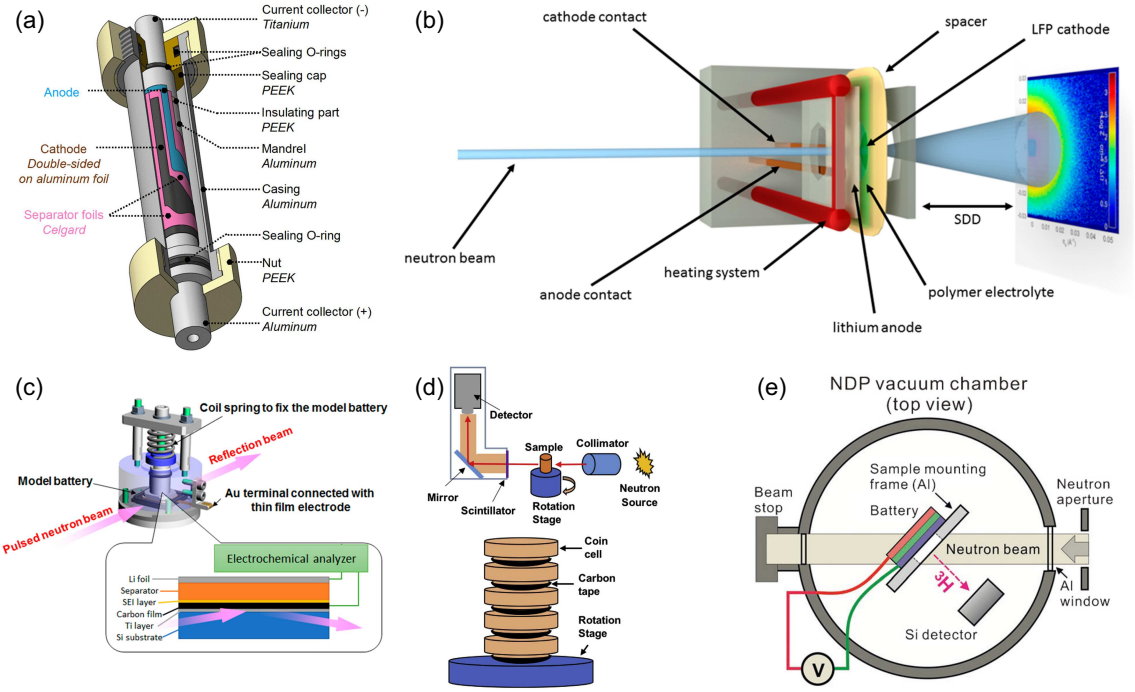


Fig. 9. (a) Cylindrical cell design for *operando* NPD experiments. Reproduced under the terms of the CC-BY 4.0 Creative Commons Attribution License (https: //creativecommons.org/licenses/by/4.0/).[151] Copyright 2018, the authors. Published by Frontiers. (b) Schematic of the full battery *operando* SANS setup with the battery components, contacts, and heating unit. Reproduced with permission.[90] Copyright 2018, American Chemical Society. (c) Schematic illustration of the electrochemical cell and cross-section of the model battery system for *in situ* NR measurements. Reproduced with permission.[99] Copyright 2016, American Chemical Society. (d) Schematic for the NI setup as well as the sample arrangement during characterization. Reproduced with permission.[118] Copyright 2018, Elsevier. (e) Schematic of the experimental setup for *operando* NDP. Reproduced with permission.[124] Copyright 2014, Wiley-VCH Verlag GmbH & Co. KGaA.

4.2. The *in situ* SANS

To conduct the *in situ* SANS experiment, Möhl *et al.* developed a special *in situ* cell setup.[90] As shown in Fig. 9(b), the *in situ* cell was assembled by laminating the lithium anode, deuterated solid polymer electrolyte, and composite cathode. A disc of 1 cm^2 working battery area was confined by a polyethylene spacer before the cell was sealed in an aluminum bag under dry Ar gas atmosphere. In the meantime, the cell was placed in an aluminum-made heating system, allowing for controlling the temperature of the cell. Based on this design, the researchers obtained the high-quality *in situ* SANS data, and demonstrated the role of single-ion diblock copolymer electrolytes in developing safer Li-metal batteries.[90] Also, for the exploration of SEI evolution, Bridges *et al.* and Sacci *et al.* designed a coin-type cell for *in situ* SANS measurements.[83,87] The overall assemble process of the *in situ* cell was similar to that of the lab coin cell.[87] Specially constructed holders were employed to locate the coin cells in

the neutron beam and provide electrical contact for the electrochemical cycling.[83] A neutron aperture was meanwhile used to locate the beam at the center of the *in situ* cell setup. In addition, pouch bag type cells with stacked electrodes and separators were also used for *in situ* SANS measurements.[162] Other optimization strategies, such as Ti–Zr alloy windows, deuterated electrolyte, to improve the quality of the SANS data were commonly used in the *in situ* SANS experiments.[84]

4.3. The *in situ* NR

A thin film electrode or thin film cell is usually needed to be constructed for *in situ* NR measurements. As shown in Fig. 9(c), to study the SEI formation during battery operation, a carbon/titanium multilayer thin film on a 3 mm thick silicon substrate with an area of 30×30 mm was used as the working electrode.[99] A magnetron sputtering method was applied to deposit a 20 nm titanium adhesion layer and a 70 nm carbon layer on the flat silicon wafer to construct the *in situ* cell.[99] In addition, a three-electrode design for *in situ* NR measurements was reported in several research works.[106,107,163] For instance, in the research work conducted by Jerliu *et al.*, a closed three-electrode electrochemical cell setup was assembled by using a ~ 40 nm thick amorphous silicon layer deposited on a 1 cm thick quartz substrate as the working electrode and lithium metal as the counter electrode and reference electrode.[107] Owejan *et al.* designed a lithium half-cell, in which lithium acted as both counter and reference electrode, for *in situ* NR experiments.[95] Considering that the specular neutron reflectivity averages over in-plane characteristic, they used copper, which was deposited onto a Ti adhesion layer on a single-crystal Si substrate, rather than graphite with a rough surface, as the working electrode.[95] Furthermore, to reduce the dominating effects of the electrode–substrate contrast and improve the sensitivity of NR to the SEI, Lee *et al.* modified the *in situ* cell based on their prior work by using a tungsten as the working electrode.[95,102]

4.4. The *in situ* NI

As an important NI method, neutron computed tomography and 3D volume visualization have been widely reported,[118,119] and figure 9(d) shows the typical NI setup as well as the cross-sectional view of sample arrangement inside Al canister.[118] To achieve the volume reconstruction, the sample was mounted on a stage which rotated through 180° to collect hundreds of or even thousands of projections. To achieve the *in situ* Bragg-edge imaging, Kamiyama *et al.* employed a lamination-type product, which consisted of a set of four layers: the negative electrode (110 μm thickness graphite), a separator (20 μm thickness microporous polyethylene), the positive electrode (116 μm thickness $LiFePO_4$), and a second separator.[123] For other *in situ* NI measurements, coin-type cells or pouch-type cells were commonly used.[113,114,120] For instance, Knoche *et al.* designed a pouch bag cell consisted of four cathode sheets, five anode sheets, and a z-folded polyethylene separator,[114] while the pouch cell used in the research conducted by Siegel *et al.* consisted of alternating double-sided current collectors.[113] Usually, a coin-type cell is not optimal for through-plane NI because that the circular geometry would complicate the data analysis and stainless-steel casing would affect the neutron transmission.[117] In order to overcome these problems, Owejan *et al.* designed a special *in situ* cell which possessed a rectangular active geometry and a neutron transparent polytetraflouroethylene (PTFE) casing.[117]

4.5. The *in situ* NDP

For *in situ* NDP measurements, a microcell or thin film battery is often fabricated by sputtering and e-beam evaporation methods.[124,126,133] The prepared cell is usually placed inside the NDP vacuum chamber and connected to a combined potentiostat/galvanostat.[126,135] A typical *in situ* NDP setup and battery configuration are shown in Fig. 9(e).[137] For the specific manufacture process of the *in situ* cell, the research work conducted by Chen *et al.* can be viewed as an example.[126] They designed an all-solid-state thin film cell which included the following configuration: 200 nm sputtered Pt current collector, 550 nm sputtered $LiCoO_2$ cathode, 2.0 μm sputtered Li_3PO_4 solid-state electrolyte, 50 nm e-beam evaporated Si anode, 150 nm e-beam evaporated copper current collector, and the cell was finally sealed using packaging coatings.[126] In addition, similar to other *in situ* neutron-based characterization methods mentioned above, pouch-type cells or coin-type cells can also be used for the *in situ* NDP experiment.[127,135] Generally, the NDP measurements are operated under high vacuum conditions, which would have no effect on the *in situ* all-solid-state cell, but is not suitable for the battery containing liquid electrolytes. For the latter case, the NDP measurements were successfully designed to be performed under reduced air pressure, though which would lead to additional but marginal energy loss of the tritons and straggling on the air molecules.[127] Also, other sample environments, such as temperature-controlled aluminum plate and disc, etc., can be attached to the *in situ* cell in the NDP vacuum chamber.[136]

5. Concluding remarks and perspectives

In summary, various neutron-based characterization techniques and the related progress regrading Li-ion battery research have been reviewed. The basic working principles, characteristics, and capabilities of these neutron scattering methods, as well as their *in situ* experiment design processes are summarized and discussed (Table 1). These advanced neutron-based characterization tools largely promoted

the fundamental research and commercial application of LIBs. Specifically, numerous breakthroughs, including the electrochemical reaction mechanisms, surface/interface/bulk structure evolution of electrode materials, Li-ion conductivity behaviors, aging mechanisms of cells, etc., have been made (Table 1). These findings based on the neutron scattering experiments are able to further guide the overall-performance optimization of LIBs.

Table 1. The characteristics or capabilities of various neutron-based characterization techniques, and the obtained main research results based on these techniques.

Neutron-based techniques	Characteristics or capabilities	Main results for Li-ion battery research
NPD	(a) Explore average crystal structure for powder battery materials (b) Combine with MEM, can visualize Li-ion diffusion path in electrode/electrolyte materials (c) Easy to design *in situ* experiment relatively	Determination of the accurate pristine structure of electrode/electrolyte materials and evaluation of their structure evolution upon (de)lithiation processes
NPDF	(a) Sensitive to both local and long-range structures for powder battery materials (b) Determine structure for amorphous battery materials (c) Detect the atomic pairs variation in the real space	Revelation of the local ordered structure of electrode materials, and the observation of local oxygen lattice evolution accompanying the oxygen redox in Li-rich cathode oxides
SANS	(a) Study the microstructure evolution of battery materials (b) Detect the formation and composition of SEI layer (c) Evaluate the surface structure of electrode materials	Evaluation of the formation, composition, structure evolution of SEI layer, as well as the identification of surface structure and nanostructure of electrode materials
NR	(a) Study the structure of SEI layer (b) Reveal the electrochemical reaction mechanisms (c) Sensitive to the surface/interface structure of electrode materials	Revelation of the structure evolution of SEI layer and Li penetration behaviors, and identification of the interface structure between electrodes and electrolytes
NI	(a) Detect the macroscopic dynamic and chemical information (b) Study the electrochemical behavior of Li-ions (c) Reveal the degradation mechanisms of commercial cells (d) Understand the manufacturing process of battery	Observation of the spatial distribution and concentration evolution of Li-ions upon cycling processes, revelation of the liquid electrolyte filling process, and revelation of the aging mechanisms in commercial batteries
NDP	(a) Study the Li-ion diffusion and concentration distribution (b) Reveal the aging mechanisms of battery (c) Detect the Li plating and stripping processes	Determination of the Li-ion diffusion, concentration distribution, and reaction rates as a function of depth, observation of the aging behaviors of cell, and revelation of the Li plating/stripping behaviors in all-solid-state batteries
QENS	(a) Study the Li-ion conductivity behaviors of battery materials (b) Reveal the ionic dynamics within batteries	Revelation of the Li-ion transport behavior and ion dynamics in solid-state electrolytes, and determination of the multiple position of Li-ions in electrode materials
INS	(a) Study the lattice dynamics of battery materials (b) Detect the ionic mobility (c) Probe the surface phonon of battery materials	Revelation of the relationship between ionic mobility and lattice dynamics in solid-state electrolytes

In addition, it was observed that each neutron scattering technique has its unique advantages and disadvantages for the Li-ion battery research. For instance, NPD can precisely provide 3D atomic level structure information, but limited only for the battery materials with good crystallinity and long-range structural order. NPDF method complements the disadvantage of NPD and can analyze the local structure of battery materials, whereas it shows limited real-space resolution and is hard to distinguish multiple components. For SANS, although it can work for the structure analysis of either crystalline materials or amorphous materials, its low-resolution data are usually difficult to be interpreted. It should be noted that SANS is a powerful tool for the SEI layer structure analysis. NR is sensitive to the surface/interface structure of materials, but the required comparatively large and atomically-flat surface is the main constraint for its measurements. As a powerful imaging tool, NI can present the visualized spatial structure information for battery materials, but its spatial resolution is only on the order of micron at present. NDP with the spatial resolution of nano-scale is very sensitive to the Li-ion concentration evolution with respect to the depth of battery materials, but its working principle limits its wide application for structure analysis. Compared with elastic neutron scattering techniques, QENS and INS can provide ionic dynamic and lattice dynamic information for battery materials. However, the lower time-resolution of QENS and INS

restricts their *in situ* measurement development. Thus, it is necessary to know the limitations of each neutron-based technique and pay much attention to selecting proper methods to gain true insight in the active materials and battery cell. Furthermore, various neutron scattering methods provide characterization information at different length scales, ranging from atomic level, single crystal level, poly-crystal level, particle level to even cell level. A combination of multi neutron-based techniques can provide more comprehensive mechanism understanding for LIBs. Although there are still some intractable challenges for LIBs needed to be solved for the achievement of high-performance LIBs, it is worth believed that, with the development of advanced neutron-based characterization techniques and their continued improved resolution, more breakthroughs will be made for the Li-ion battery research.

References

[1] Tarascon J M and Armand M 2001 *Nature* **414** 359
[2] Armstrong A R and Bruce P G 1996 *Nature* **381** 499
[3] Dunn B, Kamath H and Tarascon J M 2011 *Science* **334** 928
[4] Goodenough J B and Kim Y 2010 *Chem. Mater.* **22** 587
[5] Goodenough J B and Park K S 2013 *J. Am. Chem. Soc.* **135** 1167
[6] Vetter J, Novak P, Wagner M R, Veit C, Moller K C, Besenhard J O, Winter M, Wohlfahrt-Mehrens M, Vogler C and Hammouche A 2005 *J. Power Sources* **147** 269
[7] Li H, Wang Z, Chen L and Huang X 2009 *Adv. Mater.* **21** 4593
[8] Ellis B L, Lee K T and Nazar L F 2010 *Chem. Mater.* **22** 691
[9] Zhao E, Yu X, Wang F and Li H 2017 *Sci. Chin.-Chem.* **60** 1483
[10] Shadike Z, Zhao E, Zhou Y N, Yu X, Yang Y, Hu E, Bak S, Gu L and Yang X Q 2018 *Adv. Energy Mater.* **8** 1702588
[11] Lu J, Wu T and Amine K 2017 *Nat. Energy* **2** 17011
[12] Liu D, Shadike Z, Lin R, Qian K, Li H, Li K, Wang S, Yu Q, Liu M, Ganapathy S, Qin X, Yang Q H, Wagemaker M, Kang F, Yang X Q and Li B 2019 *Adv. Mater.* **31** 1806620
[13] Zhao E, Nie K, Yu X, Hu Y S, Wang F, Xiao J, Li H and Huang X 2018 *Adv. Funct. Mater.* **28** 1707543
[14] Ren Y and Zuo X 2018 *Small Methods* **2** 1800064
[15] Rozier P and Tarascon J M 2015 *J. Electrochem. Soc.* **162** A2490
[16] Xu J, Lin F, Doeff M M and Tong W 2017 *J. Mater. Chem. A* **5** 874
[17] Zheng J, Myeong S, Cho W, Yan P, Xiao J, Wang C, Cho J and Zhang J G 2017 *Adv. Energy Mater.* **7** 1601284
[18] Zhang J N, Li Q H, Li Q, Yu X Q and Li H 2018 *Chin. Phys. B.* **27** 088202
[19] Luo F, Liu B, Zheng J, Chu G, Zhong K, Li H, Huang X and Chen L 2015 *J. Electrochem. Soc.* **162** A2509
[20] Xu K 2014 *Chem. Rev.* **114** 11503
[21] Verma P, Maire P and Novak P 2010 *Electrochim. Acta* **55** 6332
[22] Zhao E, Chen M, Hu Z, Chen D, Yang L and Xiao X 2017 *J. Power Sources* **343** 345
[23] Zhao E, Chen M, Hu Z, Xiao X and Chen D 2016 *Electrochim. Acta* **208** 64
[24] Von Cresce A and Xu K 2011 *J. Electrochem. Soc.* **158** A337
[25] Wang Y, Liu B N, Zhou G, Nie K H, Zhang J N, Yu X Q and Li H 2019 *Chin. Phys. B.* **28** 068202
[26] Lin D, Liu Y and Cui Y 2017 *Nat. Nanotechnol.* **12** 194
[27] Cheng X B, Zhang R, Zhao C Z and Zhang Q 2017 *Chem. Rev.* **117** 10403
[28] Liu J, Bao Z, Cui Y, Dufek E J, Goodenough J B, Khalifah P, Li Q, Liaw B Y, Liu P, Manthiram A, Meng Y S, Subramanian V R, Toney M F, Viswanathan V V, Whittingham M S, Xiao J, Xu W, Yang J, Yang X Q and Zhang J G 2019 *Nat. Energy* **4** 180
[29] Miura A, Rosero-Navarro N C, Sakuda A, Tadanaga K, Phuc N H H, Matsuda A, Machida N, Hayashi A and Tatsumisago M 2019 *Nat. Rev. Chem.* **3** 189
[30] Zhao E, He L, Wang B, Li X, Zhang J, Wu Y, Chen J, Zhang S, Liang T, Chen Y, Yu X, Li H, Chen L, Huang X, Chen H and Wang F 2019 *Energy Storage Mater.* **16** 354
[31] Rao R P, Gu W, Sharma N, Peterson V K, Avdeev M and Adams S 2015 *Chem. Mater.* **27** 2903
[32] Goonetilleke D, Pramudita J C, Hagan M, Al Bahri O K, Pang W K, Peterson V K, Groot J, Berg H and Sharma N 2017 *J. Power Sources* **343** 446
[33] Sharma N, Yu D H, Zhu Y, Wu Y and Peterson V K 2017 *J. Power Sources* **342** 562
[34] Delacourt C, Poizot P, Tarascon J M and Masquelier C 2005 *Nat. Mater.* **4** 254
[35] Delacourt C, Rodriguez-Carvajal J, Schmitt B, Tarascon J M and Masquelier C 2005 *Solid State Sci.* **7** 1506
[36] Nishimura S-i, Kobayashi G, Ohoyama K, Kanno R, Yashima M and Yamada A 2008 *Nat. Mater.* **7** 707
[37] Li S, Meng X, Yi Q, Antonio Alonso J, Fernandez-Diaz M T, Sun C and Wang Z L 2018 *Nano Energy* **52** 510
[38] Goonetilleke D, Faulkner T, Peterson V K and Sharma N 2018 *J. Power Sources* **394** 1
[39] Li X Y, Zhang B, Zhang Z G, He L H, Li H, Huang X J and Wang F W 2014 *Powder Diffr.* **29** 248
[40] Liu H, Zhang X, He X, Senyshyn A, Wilken A, Zhou D, Fromm O, Niehoff P, Yan B, Li J, Muehlbauer M, Wang J, Schumacher G, Paillard E, Winter M and Li J 2018 *J. Electrochem. Soc.* **165** A1886
[41] Song B, Veith G M, Park J, Yoon M, Whitfield P S, Kirkham M J, Liu J and Huq A 2019 *Chem. Mater.* **31** 124
[42] Chen M, Zhao E, Chen D, Wu M, Han S, Huang Q, Yang L, Xiao X and Hu Z 2017 *Lnorg. Chem.* **56** 8355
[43] Zhao E, Hu Z, Xie L, Chen X, Xiao X and Liu X 2015 *Rsc Adv.* **5** 31238
[44] Zhao E, Fang L, Chen M, Chen D, Huang Q, Hu Z, Yan Q B, Wu M and Xiao X 2017 *J. Mater. Chem. A* **5** 1679
[45] Li C, Kan W H, Xie H, Jiang Y, Zhao Z, Zhu C, Xia Y, Zhang J, Xu K, Mu D and Wu F 2019 *Adv. Sci.* **6** 1801406
[46] Goonetilleke D, Sharma N, Pang W K, Peterson V K, Petibon R, Li J and Dahn J R 2019 *Chem. Mater.* **31** 376
[47] Chen C J, Pang W K, Mori T, Peterson V K, Sharma N, Lee P H, Wu S H, Wang C C, Song Y F and Liu R S 2016 *J. Am. Chem. Soc.* **138** 8824
[48] Kan W H, Wei C, Chen D, Bo T, Wang B T, Zhang Y, Tian Y, Lee J S, Liu Y and Chen G 2019 *Adv. Funct. Mater.* **29** 1808294
[49] Liu J, Whitfield P S, Saccomanno M R, Bo S H, Hu E, Yu X, Bai J, Grey C P, Yang X Q and Khalifah P G 2017 *J. Am. Chem. Soc.* **139** 9192
[50] Pang W K, Peterson V K, Sharma N, Shiu J J and Wu S h 2014 *Chem. Mater.* **26** 2318
[51] Senyshyn A, Muehlbauer M J, Dolotko O and Ehrenberg H 2015 *J. Power Sources* **282** 235
[52] Laumann A, Boysen H, Bremholm M, Fehr K T, Hoelzel M and Holzapfel M 2011 *Chem. Mater.* **23** 2753
[53] Baklanova Y V, Tyutyunnik A P, Tarakina N V, Fortes A D, Maksimova L G, Korona D V and Denisova T A 2018 *J. Power Sources* **391** 26
[54] Meesala Y, Liao Y K, Jena A, Yang N H, Pang W K, Hu S F, Chang H, Liu C E, Liao S C, Chen J M, Guo X and Liu R S 2019 *J. Mater. Chem. A* **7** 8589
[55] Wagner R, Rettenwander D, Redhammer G J, Tippelt G, Sabathi G, Musso M E, Stanje B, Wilkening M, Suard E and Amthauer G 2016 *Lnorg. Chem.* **55** 12211
[56] Orera A, Larraz G, Alberto Rodriguez-Velamazan J, Campo J and Luisa Sanjuan M 2016 *Lnorg. Chem.* **55** 1324
[57] Takami T, Morita Y, Yonemura M, Ishikawa Y, Tanaka S, Mori M, Fukunaga T and Matsubara E 2018 *Acs Appl. Energy Mater.* **1** 2546
[58] Hallopeau L, Bregiroux D, Rousse G, Portehault D, Stevens P, Toussaint G and Laberty-Robert C 2018 *J. Power Sources* **378** 48
[59] Dietrich C, Weber D A, Culver S, Senyshyn A, Sedlmaier S J, Indris S, Janek J and Zeier W G 2017 *Lnorg. Chem.* **56** 6681
[60] Sedlmaier S J, Indris S, Dietrich C, Yavuz M, Draeger C, von Seggern F, Sommer H and Janek J 2017 *Chem. Mater.* **29** 1830
[61] Strauss F, Rousse G, Dalla Corte D A, Giacobbe C, Dominko R and Tarascon J M 2018 *Lnorg. Chem.* **57** 11646
[62] Hanghofer I, Redhammer G J, Rohde S, Hanzu I, Senyshyn A, Wilkening H M R and Rettenwander D 2018 *Chem. Mater.* **30** 8134
[63] Paul N, Wandt J, Seidlmayer S, Schebesta S, Muehlbauer M J, Dolotko O, Gasteiger H A and Gilles R 2017 *J. Power Sources* **345** 85
[64] Baran V, Dolotko O, Muehlbauer M J, Senyshyn A and Ehrenberg H 2018 *J. Electrochem. Soc.* **165** A1975

[65] Lee P H, Wu S H, Pang W K and Peterson V K 2018 *J. Power Sources* **374** 31

[66] Dolotko O, Senyshyn A, Muehlbauer M J, Nikolowski K, Scheiba F and Ehrenberg H 2012 *J. Electrochem. Soc.* **159** A2082

[67] Nazer N S, Yartys V A, Azib T, Latroche M, Cuevas F, Forseth S, Vie P J S, Denys R V, Sorby M H, Hauback B C, Arnberg L and Henry P F 2016 *J. Power Sources* **326** 93

[68] Bobrikov I A, Samoylova N Y, Sumnikov S V, Ivanshina O Y, Vasin R N, Beskrovnyi A I and Balagurov A M 2017 *J. Power Sources* **372** 74

[69] Boulet-Roblin L, Sheptyakov D, Borel P, Tessier C, Novak P and Villevieille C 2017 *J. Mater. Chem. A* **5** 25574

[70] Zinth V, von Lueders C, Wilhelm J, Erhard S V, Hofmann M, Seidlmayer S, Rebelo-Kornmeier J, Gan W, Jossen A and Gilles R 2017 *J. Power Sources* **361** 54

[71] Senyshyn A, Muehlbauer M J, Dolotko O, Hofmann M and Ehrenberg H 2016 *Sci. Rep.* **5** 18380

[72] Breger J, Kang K, Cabana J, Ceder G and Grey C P 2007 *J. Mater. Chem.* **17** 3167

[73] Breger J, Dupre N, Chupas P J, Lee P L, Proffen T, Parise J B and Grey C P 2005 *J. Am. Chem. Soc.* **127** 7529

[74] Zeng D, Cabana J, Breger J, Yoon W S and Grey C P 2007 *Chem. Mater.* **19** 6277

[75] Idemoto Y, Kitamura N, Ueki K, Vogel S C and Uchimoto Y 2012 *J. Electrochem. Soc.* **159** A673

[76] Idemoto Y, Ueki K and Kitamura N 2010 *Electrochemistry* **78** 475

[77] Idemoto Y, Sera Y, Ishida N and Kitamura N 2015 *Electrochemistry* **83** 879

[78] Idemoto Y, Tejima F, Ishida N and Kitamura N 2019 *J. Power Sources* **410–411** 38

[79] Zhao E, Zhang M, Wang X, Hu E, Liu J, Yu X, Olguin M, Wynn T A, Meng Y S, Page K, Wang F, Li H, Yang X Q, Huang X and Chen L 2019 *Energy Storage Mater.* **24** 384

[80] Zhao E, Li Q, Meng F, Liu J, Wang J, He L, Jiang Z, Zhang Q, Yu X, Gu L, Yang W, Li H, Wang F and Huang X 2019 *Angew. Chem. (Int. Ed. English)* **58** 4323

[81] Liu J, Olds D, Peng R, Yu L, Foo G S, Qian S, Keum J, Guiton B S, Wu Z and Page K 2017 *Chem. Mater.* **29** 5591

[82] Liu J, Yu L, Hu E, Guiton B S, Yang X Q and Page K 2018 *Lnorg. Chem.* **57** 6873

[83] Bridges C A, Sun X G, Zhao J, Paranthaman M P and Dai S 2012 *J. Phys. Chem. C* **116** 7701

[84] Jafta C J, Sun X G, Veith G M, Jensen G V, Mahurin S M, Paranthaman M P, Dai S and Bridges C A 2019 *Energy Environ. Sci.* **12** 1866

[85] Vizgalov V A, Nestler T, Trusov L A, Bobrikov I A, Ivankov O I, Avdeev M V, Motylenko M, Brendler E, Vyalikh A, Meyer D C and Itkis D M 2018 *Crystengcomm* **20** 1375

[86] Chung S Y, Choi S Y, Kim T H and Lee S 2015 *ACS Nano* **9** 850

[87] Sacci R L, Banuelos J L, Veith G M, Littrel K C, Cheng Y Q, Wildgruber C U, Jones L L, Ramirez-Cuesta A J, Rother G and Dudney N J 2015 *J. Phys. Chem. C* **119** 9816

[88] Paul N, Wetjen M, Busch S, Gasteiger H and Gilles R 2019 *J. Electrochem. Soc.* **166** A1051

[89] Bergfelt A, Rubatat L, Mogensen R, Brandell D and Bowden T 2017 *Polymer* **131** 234

[90] Moehl G E, Metwalli E, Bouchet R, Phan T N T, Cubitt R and Mueller-Buschbaum P 2018 *Acs Energy Lett.* **3** 1

[91] Borodin O, Suo L, Gobet M, Ren X, Wang F, Faraone A, Peng J, Olguin M, Schroeder M, Ding M S, Gobrogge E, Cresce A v W, Munoz S, Dura J A, Greenbaum S, Wang C and Xu K 2017 *ACS Nano* **11** 10462

[92] He X, Wang J, Wang R, Qiu B, Frielinghaus H, Niehoff P, Liu H, Stan M C, Paillard E, Winter M and Li J 2016 *J. Mater. Chem. A* **4** 7230

[93] Ferguson P P, Todd A D W and Dahn J R 2010 *Electrochem. Commun.* **12** 1041

[94] Paul N, Brumbarov J, Paul A, Chen Y, Moulin J F, Mueller-Buschbaum P, Kunze-Liebhaeuser J and Gilles R 2015 *J. Appl. Crystallogr.* **48** 444

[95] Owejan J E, Owejan J P, DeCaluwe S C and Dura J A 2012 *Chem. Mater.* **24** 2133

[96] Hueger E, Doerrer L, Rahn J, Panzner T, Stahn J, Lilienkamp G and Schmidt H 2013 *Nano Lett.* **13** 1237

[97] Seidlhofer B K, Jerliu B, Trapp M, Hueger E, Risse S, Cubitt R, Schmidt H, Steitz R and Ballauff M 2016 *ACS Nano* **10** 7458

[98] Browning J F, Baggetto L, Jungjohann K L, Wang Y, Tenhaeff W E, Keum J K, Wood D L, I I I and Veith G M 2014 *ACS Appl. Mat. Interfaces* **6** 18569

[99] Kawaura H, Harada M, Kondo Y, Kondo H, Suganuma Y, Takahashi N, Sugiyama J, Seno Y and Yamada N L 2016 *ACS Appl. Mat. Interfaces* **8** 9540

[100] Steinhauer M, Stich M, Kurniawan M, Seidlhofer B K, Trapp M, Bund A, Wagner N and Friedrich K A 2017 *ACS Appl. Mat. Interfaces* **9** 35794

[101] Jerliu B, Hueger E, Doerrer L, Seidlhofer B K, Steitz R, Horisberger M and Schmidt H 2018 *Phys. Chem. Chem. Phys.* **20** 23480

[102] Lee C H, Dura J A, LeBar A and DeCaluwe S C 2019 *J. Power Sources* **412** 725

[103] Weiss M, Seidlhofer B K, Geiss M, Geis C, Busche M R, Becker M, Vargas-Barbosa N M, Silvi L, Zeier W G, Schroeder D and Janek J 2019 *ACS Appl. Mat. Interfaces* **11** 9539

[104] Hueger E, Stahn J and Schmidt H 2015 *J. Electrochem. Soc.* **162** A7104

[105] Strauss F, Hueger E, Heitjans P, Geue T, Stahn J and Schmidt H 2016 *Energy Technol.* **4** 1582

[106] Avdeev M V, Rulev A A, Bodnarchuk V I, Ushakova E E, Petrenko V I, Gapon I V, Tomchuk O V, Matveev V A, Pleshanov N K, Kataev E Y, Yashina L V and Itkis D M 2017 *Appl. Surf. Sci.* **424** 378

[107] Jerliu B, Doerrer L, Hueger E, Borchardt G, Steitz R, Geckle U, Oberst V, Bruns M, Schneider O and Schmidt H 2013 *Phys. Chem. Chem. Phys.* **15** 7777

[108] Jerliu B, Hueger E, Horisberger M, Stahn J and Schmidt H 2017 *J. Power Sources* **359** 415

[109] Jerliu B, Hueger E, Doerrer L, Seidlhofer B K, Steitz R, Oberst V, Geckle U, Bruns M and Schmidt H 2014 *J. Phys. Chem. C* **118** 9395

[110] Minato T, Kawaura H, Hirayama M, Taminato S, Suzuki K, Yamada N L, Sugaya H, Yamamoto K, Nakanishi K, Orikasa Y, Tanida H, Kanno R, Arai H, Uchimoto Y and Ogumi Z 2016 *J. Phys. Chem. C* **120** 20082

[111] Hirayama M, Shibusawa T, Yamaguchi R, Kim K, Taminato S, Yamada N L, Yonemura M, Suzuki K and Kanno R 2016 *J. Mater. Res.* **31** 3142

[112] Taminato S, Hirayama M, Suzuki K, Kim K, Tamura K and Kanno R 2018 *J. Phys. Chem. C* **122** 16607

[113] Siegel J B, Lin X, Stefanopoulou A G, Hussey D S, Jacobson D L and Gorsich D 2011 *J. Electrochem. Soc.* **158** A523

[114] Knoche T, Zinth V, Schulz M, Schnell J, Gilles R and Reinhart G 2016 *J. Power Sources* **331** 267

[115] Kino K, Yonemura M, Ishikawa Y and Kamiyama T 2016 *Solid State Ionics* **288** 257

[116] Senyshyn A, Muehlbauer M J, Dolotko O, Hofmann M, Pirling T and Ehrenberg H 2014 *J. Power Sources* **245** 678

[117] Owejan J P, Gagliardo J J, Harris S J, Wang H, Hussey D S and Jacobson D L 2012 *Electrochim. Acta* **66** 94

[118] Zhang Y, Chandran K S R and Bilheux H Z 2018 *J. Power Sources* **376** 125

[119] Zhang Y, Chandran K S R, Jagannathan M, Bilheux H Z and Bilheux J C 2017 *J. Electrochem. Soc.* **164** A28

[120] Nie Z, McCormack P, Bilheux H Z, Bilheux J C, Robinson J P, Nanda J, Koenig G M and Jr. 2019 *J. Power Sources* **419** 127

[121] Michalak B, Sommer H, Mannes D, Kaestner A, Brezesinski T and Janek J 2015 *Sci. Rep.* **5** 15627

[122] Starke B, Seidlmayer S, Schulz M, Dinter A, Revay Z, Gilles R and Pettinger K H 2017 *J. Electrochem. Soc.* **164** A3943

[123] Kamiyama T, Narita Y, Sato H, Ohnuma M and Kiyanagi Y 2017 *Neutron Imaging for Applications in Industry and Science* (Chen D, *et al.* Ed.) p. 27

[124] Liu D X, Wang J, Pan K, Qiu J, Canova M, Cao L R and Co A C 2014 *Angew. Chem.-Int. Ed.* **53** 9498

[125] Lv S, Verhallen T, Vasileiadis A, Ooms F, Xu Y, Li Z, Li Z and Wagemaker M 2018 *Nat. Commun.* **9** 2152

[126] Chen C, Oudenhoven J F M, Danilov D L, Vezhlev E, Gao L, Li N, Mulder F M, Eichel R A and Notten P H L 2018 *Adv. Energy Mater.* **8** 1801430

[127] Liu M, Cheng Z, Qian K, Verhallen T, Wang C and Wagemaker M 2019 *Chem. Mater.* **31** 4564

[128] Zhang X, Verhallen T W, Labohm F and Wagemaker M 2015 *Adv. Energy Mater.* **5** 1500498

[129] Ceccio G, Cannavo A, Horak P, Torrisi A, Tomandl I, Hnatowicz V, Tsai H S and Vacik J 2018 *Radiat Eff. Defects Solids* **173** 836

[130] Wetjen M, Trunk M, Werner L, Gasteiger H A, Gernhaeuser R, Gilles R, Maerkisch B and Revay Z 2019 *J. Electrochem. Soc.* **166** A1408

[131] Li Q, Yi T, Wang X, Pan H, Quan B, Liang T, Guo X, Yu X, Wang H, Huang X, Chen L and Li H 2019 *Nano Energy* **63** 103895
[132] Nagpure S C, Mulligan P, Canova M and Cao L R 2014 *J. Power Sources* **248** 489
[133] Oudenhoven J F M, Labohm F, Mulder M, Niessen R A H, Mulder F M and Notten P H L 2011 *Adv. Mater.* **23** 4103
[134] Nagpure S C, Downing R G, Bhushan B, Babu S S and Cao L 2011 *Electrochim. Acta* **56** 4735
[135] Wetjen M, Trunk M, Werner L, Gernhaeuser R, Maerkisch B, Revay Z, Gilles R and Gasteiger H A 2018 *J. Electrochem. Soc.* **165** A2340
[136] Wang C, Gong Y, Dai J, Zhang L, Xie H, Pastel G, Liu B, Wachsman E, Wang H and Hu L 2017 *J. Am. Chem. Soc.* **139** 14257
[137] Han F, Westover A S, Yue J, Fan X, Wang F, Chi M, Leonard D N, Dudney N, Wang H and Wang C 2019 *Nat. Energy* **4** 187
[138] Sinha K, Wang W, Winey K I and Maranas J K 2012 *Macromolecules* **45** 4354
[139] Sacci R L, Lehmann M L, Diallo S O, Cheng Y Q, Daemen L L, Browning J F, Doucet M, Dudney N J and Veith G M 2017 *J. Phys. Chem. C* **121** 11083
[140] Muy S, Bachman J C, Giordano L, Chang H H, Abernathy D L, Bansal D, Delaire O, Hori S, Kanno R, Maglia F, Lupart S, Lamp P and Shao-Horn Y 2018 *Energy Environ. Sci.* **11** 850
[141] Ganapatibhotla L V N R and Maranas J K 2014 *Macromolecules* **47** 3625
[142] Nozaki H, Harada M, Ohta S, Watanabe I, Miyake Y, Ikedo Y, Jalarvo N H, Mamontov E and Sugiyama J 2014 *Solid State Ionics* **262** 585
[143] Lefevr J, Cervini L, Griffin J M and Blanchard D 2018 *J. Phys. Chem. C* **122** 15264
[144] Wagemaker M, Kearley G J, van Well A A, Mutka H and Mulder F M 2003 *J. Am. Chem. Soc.* **125** 840
[145] Wagemaker M, van Well A A, Kearley G J and Mulder F M 2004 *Solid State Ionics* **175** 191
[146] Heitmann T, Hester G and Mitra S 2018 *Physica B* **551** 315
[147] Singh B, Gupta M K, Mittal R, Zbiri M, Rols S, Patwe S J, Achary S N, Schober H, Tyagi A K and Chaplot S L 2017 *Phys. Chem. Chem. Phys.* **19** 15512
[148] Benedek P, Yazdani N, Chen H, Wenzler N, Juranyi F, Månsson M, Islam M S and Wood V C 2019 *Sustainable Energy & Fuels* **3** 508
[149] Xie Y, Naguib M, Mochalin V N, Barsoum M W, Gogotsi Y, Yu X, Nam K W, Yang X Q, Kolesnikov A I and Kent P R C 2014 *J. Am. Chem. Soc.* **136** 6385
[150] Papanek P, Kamitakahara W A, Zhou P and Fischer J E 2001 *J. Phys.: Condens. Matter* **13** 8287
[151] Vitoux L, Reichardt M, Sallard S, Novák P, Sheptyakov D and Villevieille C 2018 *Front. Energy Res.* **6** 76
[152] Bergstom O, Andersson A M, Edstrom K and Gustafsson T 1998 *J. Appl. Crystallogr.* **31** 823
[153] Rosciano F, Holzapfel M, Scheifele W and Novak P 2008 *J. Appl. Crystallogr.* **41** 690
[154] Godbole V A, Heß M, Villevieille C, Kaiser H, Colin J F and Novák P 2013 *RSC Adv.* **3** 757
[155] Bianchini M, Leriche J B, Laborier J L, Gendrin L, Suard E, Croguennec L and Masquelier C 2013 *J. Electrochem. Soc.* **160** A2176
[156] Sharma N, Du G, Studer A J, Guo Z and Peterson V K 2011 *Solid State Ionics* **199-200** 37
[157] Roberts M, Biendicho J J, Hull S, Beran P, Gustafsson T, Svensson G and Edström K 2013 *J. Power Sources* **226** 249
[158] Brant W R, Roberts M, Gustafsson T, Biendicho J J, Hull S, Ehrenberg H, Edström K and Schmid S 2016 *J. Power Sources* **336** 279
[159] Pang W K and Peterson V K 2015 *J. Appl. Crystallogr.* **48** 280
[160] Liu H, Fell C R, An K, Cai L and Meng Y S 2013 *J. Power Sources* **240** 772
[161] Vadlamani B, An K, Jagannathan M and Chandran K S R 2014 *J. Electrochem. Soc.* **161** A1731
[162] Seidlmayer S, Hattendorff J, Buchberger I, Karge L, Gasteiger H A and Gilles R 2015 *J. Electrochem. Soc.* **162** A3116
[163] DeCaluwe S C, Dhar B M, Huang L, He Y, Yang K, Owejan J P, Zhao Y, Talin A A, Dura J A and Wang H 2015 *Phys. Chem. Chem. Phys.* **17** 11301